R. & M. No. 3656

MINISTRY OF AVIATION SUPPLY
AERONAUTICAL RESEARCH COUNCIL
REPORTS AND MEMORANDA

On the Static Performance of Two-Dimensional Intakes with Momentum Injection in the Form of Boundary-Layer Control by Blowing

By N. GREGORY

Aerodynamics Division N.P.L.

LONDON: HER MAJESTY'S STATIONERY OFFICE
1971
PRICE £1 10*s* 0*d* [£1·50] NET

On the Static Performance of Two-Dimensional Intakes with Momentum Injection in the Form of Boundary-Layer Control by Blowing

By N. GREGORY

Aerodynamics Division N.P.L.

Reports and Memoranda No. 3656*
February, 1968

Summary.

A theoretical one-dimensional analysis has been used to calculate at zero forward speed the static pressure and total-pressure recovery far down the throat of two-dimensional intakes in terms of the mean inflow rate (or Mach number), the mean pressure on the forward-facing lip and the coefficient of contraction of the intake. Total pressure is lost at high mass flows with thin-lipped intakes, as it is impossible to satisfy the momentum equation with the intake running full and flow separation occurs. At a given intake Mach number, the lower the mean lip pressure that can be generated by the flow, the higher the total-pressure recovery and the mass flow, a return which diminishes with decreasing lip thickness.

At a given intake Mach number, the effect of air injection at a downstream facing slot depends on its effect on the flow geometry. If the lip static pressure remains constant or changes only with the mass flow, the improvement in total-pressure recovery or in mass flow is in theory small and in practice the gains are outweighed by increased viscous losses associated with the blowing. In theory, a distinction must be drawn, however, between the above type of flow separation where it is impossible for the given mass flow to run full, and that which occurs because of regions where the pressure gradient would be severely adverse in inviscid flow running full. Here boundary-layer control by blowing might be expected to eliminate separation, and the resulting change in flow geometry to allow decreases in lip pressure and consequent greater improvements in pressure recovery and in choking mass-flow rates.

An incompressible-flow design method is presented for calculating the shape of intakes in which the curved lip is a constant-pressure surface and is followed by a local region of adverse pressure gradient. Three intakes with differing coefficients of contraction were made and tested with boundary-layer control by blowing applied downstream of the lip.

The experiments reveal the existence of a narrow range of contraction ratios and inflow rates of practical importance where blowing prevents separation, and critical blowing mass-flow and momentum-flux ratios were established experimentally, the latter quantity being independent of slot width. It was found that with a narrow slot the maximum efficiency of total-pressure recovery obtained (representing increases of up to 2 per cent over the efficiency without blowing) occurred at blowing rates between one third and one half of the critical because the mixing losses are high. With a wider slot, the maximum efficiency occurred close to the critical blowing rate, but tests are needed for a complete assessment of optimum conditions, which may not coincide with the point of elimination of separation. Surprisingly, even at flow rates where attached flow was impossible from momentum considerations, strong blowing reduced the extent of separation enough to improve intake efficiency.

The theoretical analysis assumed that shock waves and associated losses did not occur. The experimental work revealed that patches of supersonic flow on the lip were possible without shock waves, suggesting that further improvements might result from lip shape modifications aimed at achieving a definite measure of isentropic recompression.

*Replaces NPL Aero Special Report 006 – A.R.C. 29 888.

LIST OF CONTENTS

1. *Introduction.*

The advent of V.T.O.L. has introduced further complications into the design of air intakes for jet engines. Where the same forward-facing intake and engine are used to supply thrust for both propulsion and lifting purposes, high intake efficiency becomes even more important at zero forward speed than it already is at high forward speeds. Now it is desirable to keep the external dimensions of an intake as small as possible, with a thin lip, in order to minimise the drag at high forward speed, yet the penalties for operating a thin-lipped intake near choking at zero and low forward speeds are severe. It is well known that such an intake does not run full in these circumstances, for it is impossible to satisfy the momentum equation with the flow remaining attached. In the extreme case of a sharp lip at zero forward speed[1], the total-pressure recovery and mass-flow ratios are each 0·79 for a choked inlet compared with 1·00 ideally attainable with an inlet with large lip radius.

Attached flow in these examples could require surface pressures even less than complete vacuum*, which is impossible, and in the real flow with *vena contracta*, the separation is found to take place because the boundary-layer cannot withstand the adverse pressure gradient along the surface which accompanies the pattern of separated flow. But there are also intake shapes and flow rates in which the real flow separates, but where there is no physical objection to the intake running full were it not for the effect on the boundary layer of the adverse pressure gradient which would then obtain.

In these latter cases, established means of boundary-layer control might be expected to prevent separation and to minimise total-pressure loss. In the former case the effect of boundary-layer control is less obvious, and this is in part the reason for the present exploratory work.

The alternatives facing the V.T.O.L. designer who cannot afford unnecessary loss at zero forward speed appeared to be either a thin lip which necessarily separates in these conditions and to take additional measures such as variable geometry or auxiliary air inlets for preventing or minimising the losses, or else to find the thinnest lip which can run full, using boundary-layer control techniques if necessary to ensure that it does. The present work, however, shows that boundary-layer control by blowing has some beneficial effect even in the first case. The investigation was inspired by a suggestion put forward by Dr. E. J. Gabbay[2] that boundary-layer control by blowing might have some advantages over suction in this problem. Entrainment could lead to increased mass flow at choking.

An 'optimum' contour for intakes has been defined by Küchemann and Weber[3] as one whose shape is such as to minimise and maintain constant the velocity over the forward-facing external surface on the grounds that this leads to the highest critical Mach number at which shock waves and drag rise can be expected. Dr. Gabbay[12] suggested that a corresponding 'optimum' contour for a two-dimensional intake designed for zero forward speed had constant velocity over the whole forward-facing portion of its surface so as to maximise the lip suction for a given peak value of surface velocity and lip thickness. However, following the development of the concept[11] that the onset of shock waves and drag rise on aerofoils can be postponed if the contour can be designed so that the patch of supersonic flow that develops with increasing free-stream Mach number is terminated by isentropic recompression instead of by a shock wave, it may be questioned whether the concept of 'optimum' contour just defined necessarily leads to an intake of given lip thickness that accepts the greatest mass inflow without loss. Nevertheless it was thought worthwhile to design three two-dimensional intake shapes for differing ratios of velocity on curved lip to velocity far down the intake, to incorporate a slot for boundary-layer control by blowing at the downstream end of the curved lip inside the intake, and to test them with blowing in an attempt to avoid flow separation in the ensuing region of adverse pressure gradient.

The experimental work emphasizes another complicating feature which should be mentioned at this stage. As compressibility effects come into prominence with increasing mass flow into the intake, the shape of the pressure distribution changes. The intakes were designed by an incompressible flow method, however, so the pressure is no longer constant on the curved lip for the intake mass flows in the range of interest.

This report, then, starts in Section 2 with a discussion on a one-dimensional basis of the theoretical

*Quite apart from this, long before the mass flow reached these levels, losses would have resulted from shock waves terminating regions of supersonic flow over the lip.

performance characteristics of intakes with shock-free flow, and indicates the limits beyond which separation, and hence losses, become unavoidable. The effect of downstream injection of momentum is also considered. In Section 3, the incompressible-flow method is given for designing intakes with constant pressure lips. The tests carried out at zero forward speed on three such intakes are described in Section 5, and the experimental work is summed up and conclusions are drawn in Section 6.

2. *Theoretical Performance Characteristics of 'Optimum' Intakes.*

Consider the class of 'optimum' intakes illustrated in Fig. 1. This two-dimensional parallel-sided intake has a coefficient of contraction defined by $C = h/(h+t)$ and the expression 'optimum' implies that the suction force on the forward-facing lip has been maximised for a given peak velocity as the flow is assumed to possess this velocity U_2 and the associated pressure p_2 over the whole of the curved portion of the lip. The design of such an intake will be discussed in the next Section, but it should be remembered that though an intake of given contraction ratio designed by incompressible-flow theory will yield a constant pressure coefficient over the lip at low intake Mach numbers M_1, this will cease to be true as the Mach number rises, because of compressibility effects. Thus in calculating and discussing the general performance of optimum intakes over a range of inlet Mach number we are allowing the intake shape to vary with Mach number, even at a fixed contraction ratio: a real intake must be designed for the specific inlet Mach number at which it is required to operate with maximum efficiency.

At the downstream end of the curved lip a flush slot is incorporated with throat width d, and is connected to an air supply having stagnation pressure and temperature p_3 and $\overline{T}_3$ respectively*. The axis of the slot is assumed to lie at a very small angle to the axis of the intake.

Now consider the static flow into the intake, neglecting displacement effects and total-pressure losses due to the growth of boundary layers on the walls. The analysis takes the form of a generalization to non-zero lip thickness, and an extension to permit air injection, of the one-dimensional analysis given by Fradenburgh and Wyatt[1].

Assume that the stagnation pressure of the blown air, P_3, is sufficient to choke the slot and that this air expands isentropically to local static pressure p_2. At the slot throat, of width d, $M = 1$ and therefore

$$\rho = \rho_3 \left(\frac{2}{\gamma+1} \right)^{\frac{1}{\gamma-1}}$$

and

$$U = \bar{a}_3 \left(\frac{2}{\gamma+1} \right)^{\frac{1}{2}}.$$

The mass flow of the injected air is therefore given by

$$m_3 = \rho U d = \rho_3 \bar{a}_3 d \left(\frac{2}{\gamma+1} \right)^{\frac{1+\gamma}{2(\gamma-1)}}. \tag{1}$$

At station (2), the slot exit,

$$U_2 = M_2 \bar{a}_3 \left(\frac{2}{2+(\gamma-1) M_2^2} \right)^{\frac{1}{2}},$$

*In the case of temperature (T) and speed of sound (a), the bar is used to indicate local stagnation conditions.

where M_2 is given by

$$\frac{p_2}{P_3} = \left(\frac{2}{2+(\gamma-1)M_2^2}\right)^{\frac{\gamma}{\gamma-1}}$$

so that the momentum of the ejected air is given by

$$m_3 U_2 = \gamma d P_3 \left(\frac{2}{\gamma+1}\right)^{\frac{1+\gamma}{2(\gamma-1)}} \sqrt{\frac{2}{\gamma-1}\left[1-\left(\frac{p_2}{P_3}\right)^{\frac{\gamma-1}{\gamma}}\right]}, \tag{2}$$

using the equation for the stagnation speed of sound,

$$\bar{a}^2 \rho = \gamma P. \tag{3}$$

The equations for conservation of mass flow and of energy state that

$$m_0 + m_3 = m_1 \tag{4}$$

and

$$m_0 C_p \overline{T}_0 + m_3 C_p \overline{T}_3 = m_1 C_p \overline{T}_1. \tag{5}$$

If it is assumed that $\overline{T}_3 = \overline{T}_0$, as is the case in the wind-tunnel tests, these equations determine that $\overline{T}_1$ is also equal to $\overline{T}_0$. This implies that

$$\bar{a}_3 = \bar{a}_1 = \bar{a}_0. \tag{6}$$

This result can be justified *a posteriori* even for the flight application since it remains very closely true for the compression ratios and blowing mass-flow ratios found to be of practical importance.

The mass flow far down the intake is given by

$$m_1 = \rho_1 U_1 h = \frac{\gamma p_1 h}{\bar{a}_0}\left(\frac{M}{a/\bar{a}}\right)_1 \tag{7}$$

using equation (6) and the equation for the local speed of sound,

$$a^2 \rho = \gamma p. \tag{8}$$

A reference mass flow m^* may be defined as the choking flow ($M_1 = 1$) at free-stream total pressure across the inlet throat, h. That is,

$$\begin{aligned} m^* &= \frac{\gamma P_0 h}{\bar{a}_0}\left(\frac{p}{P}\right)_{M=1}\left(\frac{M}{a/\bar{a}}\right)_{M=1} \\ &= \frac{\gamma P_0 h}{\bar{a}_0}\left(\frac{2}{\gamma+1}\right)^{\frac{1+\gamma}{2(\gamma-1)}}. \end{aligned} \tag{9}$$

An alternative reference flow is

$$m' = m^*/C, \tag{10}$$

that is, the choking flow across the total height of the inlet, $h+t$.

Dimensionless forms of the mass flow far down the intake and of the blowing rate are therefore obtained from (7) and (9),

$$\frac{m_1}{m'} = C\left(\frac{p}{P}\right)_1\left(\frac{P_1}{P_0}\right)\left(\frac{M}{a/\bar{a}}\right)_1\left(\frac{\gamma+1}{2}\right)^{\frac{1+\gamma}{2(\gamma-1)}} \tag{11}$$

and from (1) and (9),

$$\frac{m_3}{m'} = \left(\frac{d}{h}\right)\left(\frac{P_3}{P_0}\right)C. \tag{12}$$

Equation (12) may be divided by equation (11) to give the blowing mass flow as a proportion of the total flow,

$$\frac{m_3}{m_1} = \left(\frac{d}{h}\right)\left(\frac{P_3}{P_0}\right)\left(\frac{a}{\bar{a}}\right)_1 M_1\left(\frac{p}{P}\right)_1\left(\frac{P_1}{P_0}\right)\left(\frac{\gamma+1}{2}\right)^{\frac{\gamma+1}{2(\gamma-1)}}. \tag{13}$$

The momentum equation for components parallel to the flat surfaces of the intakes states that

$$(p_0-p_2)\,t+(p_0-p_1)\,h = \rho_1 U_1^2 h - m_3 U_2 \tag{14}$$

since the contribution of pressure on, and momentum flux across external sections far removed from the intake mouth are both zero. Note that this equation is not restricted to 'optimum' intakes for it remains generally true with p_2 bearing the interpretation of mean pressure across the thickness of the lip. With the aid of equation (8), equation (14) may be re-written in the form

$$\left(1-\frac{p_2}{P_0}\right)\frac{t}{h}+\left(1-\frac{p_1}{P_0}\right) = \frac{p_1}{P_0}\gamma M_1^2 - \frac{m_3 U_2}{P_0 h},$$

whence re-arranging and using equation (2), the total-pressure recovery and static pressure far downstream are given by the following equations,

$$\frac{P_1}{P_0} = \frac{1}{(\gamma M_1^2+1)\left(\frac{p}{P}\right)_1}\left\{\frac{1}{C}-\frac{1-C}{C}\left(\frac{p_2}{P_0}\right)+\gamma\left(\frac{d}{h}\right)\left(\frac{P_3}{P_0}\right)\left(\frac{2}{\gamma+1}\right)^{\frac{1+\gamma}{2(\gamma-1)}}\right.$$
$$\left.\sqrt{\frac{2}{\gamma-1}\left[1-\left(\frac{p_2/P_0}{P_3/P_0}\right)^{\frac{\gamma-1}{\gamma}}\right]}\right\} \tag{15}$$

$$\frac{p_1}{P_0} = \left(\frac{P_1}{P_0}\right)\left(\frac{p}{P}\right)_1. \tag{16}$$

If the coefficient of contraction of an intake C and the suction on the lip p_2/P_0 are specified, and the slot width d/h and blowing pressure ratio P_3/P_0 are also known, equation (15) gives the total pressure far downstream, equation (16) the static pressure, equation (11) the mass-flow ratio and equation (13) the blowing mass-flow ratio, all in terms of M_1 the Mach number far down the intake which determines $(p/P)_1$ and $(a/\bar{a})_1$. In the absence of a blowing slot, m_3 is zero, equation (13), and the last term in brackets in equation (15) is also zero. The other relations are not affected.

Equation (15) contains (p_2/P_0) the mean pressure over the lip of the intake as an undetermined para-

meter which is in fact fixed by the geometry of the flow (with or without separation) and the inlet Mach number. Consequently, inadmissible values of P_1/P_0 may be predicted if inappropriate values of p_2/P_0 are chosen. An overriding limitation on P_1/P_0 is set by the fact that the entropy cannot decrease. Since the stagnation temperature is constant thoughout the flow this limitation implies that without blowing, $P_1/P_0 \leqslant 1$, and with blowing $P_1/P_0 \leqslant (P_3/P_0)^{m_3/m_1}$, (*see* Appendix I). Further limitations are imposed by the restrictions that p_2/P_0 cannot exceed 1 or be negative. A zero value implies infinite Mach number on the curved lip but long before this value is reached the present analysis breaks down on account of additional losses due to shock waves†. However it may be that modifications to the contour to contrive shock-free isentropic compression could permit mean lip pressures well below the same value (i.e., the value $p_2/P_0 = 0{\cdot}528$ corresponding to sonic velocity): the present idealised theoretical analysis has therefore been carried out for lip pressures right down to zero.

For the case without blowing, values of total and static pressure far down the intake are shown in Figs. 2 (a–f), as functions of mass-flow ratio, m_1/m', and lip pressure ratio, p_2/P_0, for contraction coefficient values of 0·50, 0·67, 0·80, 0·89, 0·94 and 1·0. In addition to the contours of constant p_2/P_0 shown on these Figures, contours of constant downstream Mach number M_1 are also given. The intake total pressure has been cross-plotted in Figs. 3 (a–c) as a function of mass-flow ratio and coefficient of contraction for various lip pressures. Since boundary-layer losses have been neglected in this theory, the total-pressure recovery will in reality be somewhat less than as shown, but even so, it can be seen from Figs. 2 and 3 that for a given minimum lip-pressure ratio, full total-pressure recovery is only possible up to certain mass-flow rates. Above these flow rates, it is impossible to balance the momentum relation. The flow therefore detaches from the surface, and following a *vena contracta*, total pressure is lost in the expansion to fill the intake further downstream. The change with increasing mass-flow from no loss to loss of total pressure is also accompanied (Fig. 2) by a change of slope in the downstream static-pressure curve. Note that with the thinner lipped intakes the flow rate above which a loss of total pressure would occur, even if complete vacuum could be obtained on the lips, is quite low.

Flow separation is thus seen to occur in a hypothetical inviscid flow; and in a real viscous flow, boundary-layer control by suction would not be expected to prevent it. Boundary-layer control by blowing, however, introduces momentum which, as is already seen from equations (14) and (15), reduces the forward thrust required from the lip suction, other things being equal, and therefore might be expected to be a little more effective than suction in balancing the momentum equation and thus in preventing separation on this account at these high inflow rates.

The maximum flow rate for loss-free flow is less than the choking flow rate for contraction coefficients above 0·789 (i.e. intakes with thin lips), and these flow rates are plotted as functions of contraction coefficient in Fig. 4 together with the associated values of lip pressure ratio and inlet Mach number. The mass flows have been non-dimensionalized both in terms of m', the choking flow at intake total pressure through the overall intake height, $h+t$, and of m^*, the corresponding flow through the throat height, h. It will be noted that for contraction ratios above 0·789, the maximum flow with or without losses requires, according to our theory, the unrealistic lip pressure of zero, i.e. vacuum. For comparison, therefore, the slightly reduced flows that are obtainable when the lip pressure ratio is restricted to 0·528, the sonic value, are shown in Fig. 5. For an intake with fixed overall thickness, $h+t$, it will be seen that the contraction coefficient for maximum loss-free flow rate has been reduced from 0·789 to 0·638.

For intakes with boundary-layer control by blowing through a slot, the induction effect of blowing (i.e. the increase in mass-flow rate due to blowing) can be examined only in a selection of cases, since two additional parameters are introduced, slot width d/h and blowing pressure P_3/P_0. Values of $d/h = 0{\cdot}0033$ and $P_3/P_0 = 5$ have been taken and the performance curves for intakes with contraction coefficients of 0·67, 0·80 and 0·89 are shown in Figs. 6 (a, b, c), which may be compared with the corresponding Figs. 2 (b, c, d), for the results without blowing.

The performance of intakes with blowing under other conditions can rapidly be estimated from the

---

†A more comprehensive one-dimensional analysis admitting supersonic secondary flow, and with application to ejectors, has been given by Hanbury[14].

results given in Fig. 2 (a–f) without blowing since equations (15), (16), (11) and (12) show that *at the same downstream Mach number M_1 and lip pressure p_2/P_0,*

$$\frac{\left(\frac{P_1}{P_0}\right)}{\left(\frac{P_1}{P_0}\right)_{\text{no blow}}} = \frac{\left(\frac{p_1}{P_0}\right)}{\left(\frac{p_1}{P_0}\right)_{\text{no blow}}} = \frac{\left(\frac{m_1}{m'}\right)}{\left(\frac{m_1}{m'}\right)_{\text{no blow}}} = 1+G$$

where

$$G = \frac{\gamma\left(\frac{d}{h}\right)\left(\frac{P_3}{P_0}\right)\left(\frac{2}{\gamma+1}\right)^{\frac{1+\gamma}{2(\gamma-1)}}\sqrt{\frac{2}{\gamma-1}\left[1-\left(\frac{p_2/P_0}{P_3/P_0}\right)^{\frac{\gamma-1}{\gamma}}\right]}}{\frac{1}{C}-\frac{1-C}{C}\left(\frac{p_2}{P_0}\right)} \tag{17}$$

and

$$\frac{m_3}{m'} = \left(\frac{d}{h}\right)\left(\frac{P_3}{P_0}\right)C. \tag{12}$$

Note that G and $\frac{m_3}{m'}$ are proportional to d/h. A value of 10^{-2} for d/h has been selected and tables of G and $\frac{m_3}{m'}$ are given for a range of pressure ratios of interest, for contraction ratios of 0·67, 0·80, 0·89 and 1·0 in Table 1. The maximum values of P_1/P_0 are either determined by the condition $p_2/P_0 = 0$ (or by any more realistic higher limit that might be chosen) or are equal to $(P_3/P_0)^{m_3/m_1}$ (Appendix I), whichever gives the lower value of P_1/P_0.

The graphs shown in Fig. 6 (a–c) have not been extended to zero values of m_1/m' partly because this is a region of little interest and partly because the blowing has been taken at constant values of d/h and P_3/P_0 so that the mass-flow injected m_3/m' has been a constant. In practice, if the injected air were supplied by the compressor fitted to the intake, the injected air m_3/m' would be proportional to m_1/m'. The present calculations have been restricted to inflow rates for which the blowing rate m_3/m' remains less than 10 per cent.

Since the downstream Mach number, and hence velocity, have been kept constant in the condition leading to equations (17), the ratio of either mass, momentum or energy flux with blowing to that without blowing is equal to $1+G$. But it is assumed that m_3 is removed for blowing so that the mass-flow ratio available downstream of the compressor for the later engine stages is

$$\left(\frac{m_1-m_3}{m_1}\right)_{\text{no blow}} = 1+G-\frac{\frac{m_3}{m'}}{\left(\frac{m_1}{m'}\right)_{\text{no blow}}}.$$

A study of Fig. 6 (a–c) and of Table 1 shows that this ratio can be either greater or less than unity. An increase in available mass-flow is achieved if the no-blow inflow rate exceeds a value lying between 0·5 and 0·9 of m', and this break-even value is reduced by decrease in coefficient of contraction, by reduction in mean lip pressure and by increase in blowing pressure ratio, though this latter effect is reduced to zero when the lip pressure also reaches zero. The greatest gains in available mass-flow occur at choking and

with the lowest realisable lip pressure, but are only in the region of 1/3 to 1/2 of the value of $\frac{m_3}{m'}$, and so are not very large. The gain in total-pressure recovery $1+G$, is somewhat greater, and positive at all downstream Mach numbers, but is of course paid for in the work done to compress the blowing air. Further consideration of this would require knowledge of the thermodynamic efficiency of the engine compressor.

It thus appears that even when viscous effects (i.e. skin-friction and mixing losses) are neglected, only small gains in mass-flow are possible by air injection into an intake when the flow is unseparated (i.e. loss free), or when the geometry of the flow is determined solely by momentum considerations. The main scope for blowing would therefore seem to lie in controlling the boundary layer and in preventing separation in the limited range of conditions where this is due to the adverse pressure gradient associated with unseparated flow, and the change in flow geometry allows changes in the lip pressure p_2/P_0. This aspect of blowing is examined experimentally in Section 4.

3. *Design of 'Optimum' Intakes.*

The design of optimum intakes in incompressible flow can be carried out by a series of conformal transformations. The planes used are illustrated in Fig. 7. The intake, illustrated in the z-plane, is slightly more general than that already referred to in that the surface ED along which the velocity rises from zero to U_2 at D is inclined at an angle θ_0 to the parallel portion of the intake CB; this angle is negative and may take values between $-\pi$ and 0. The velocity along the constant-pressure (free-streamline) surface DC is U_1, and along the flat surface CB the velocity falls from U_2 to $U_1 = 1$.

The intake thus differs slightly from the 'optimum' when θ is not equal to $-\pi$ as its overall thickness is not limited and is greater than the distance between D and AB, but the velocity falls off to zero very rapidly along DE so that the contribution of the pressures acting on DE to the overall forward component of pressure acting on BCDE is a small one for values of θ close to $-\pi$. It was therefore not unexpected that comparisons between calculated intake shapes with DE making both $-175°$ and $-180°$ with CB showed that the change in the contour of DC was small and was confined to the region close to D. Thus, the small slope of DE allows the outer contour to be more easily faired into a shape designed for forward speed conditions, yet these intakes may be treated as if they were 'optimum' ones.

The class of intakes bears a close similarity to a series of nozzles discussed by Gabbay[4], and to a series of lifting engine intakes discussed by Barche[13].

The intakes may be quickly designed, to an accuracy determined by the quality of equipment used, by means of the rheo-electric analogy on the lines set out by Cahn[5].

We set $U_1 = 1$ in the z-plane, and since $u = \frac{\partial \phi}{\partial x} = \frac{\partial \psi}{\partial y}$, we note that if AB is $\psi = 0, \psi_s = h$ along BC, and far down BB, $\frac{\partial \phi}{\partial x} = 1$. Along CD in the z-plane, we have

$$\partial s = \frac{1}{U_2} \partial \phi .$$

But $dx = ds \cos\theta$ and $dy = ds \sin\theta$, so that the intake ordinates are given parametrically by

$$\frac{x}{h} = -\frac{1}{U_2 h} \int_c \cos\theta \, d\phi \tag{18}$$

and

$$\frac{y}{h} = -\frac{1}{U_2 h} \int_c \sin\theta \, d\phi . \tag{19}$$

The functional relation $\theta = f(\phi)$ along CD remains the same in the log-hodograph or Q-plane and this function can be determined experimentally by cutting out a long narrow strip of electrically conducting paper of uniform resistance (e.g. 'Teledeltos' paper) and applying a potential difference between a distant terminal AE and the point B. It can be shown that the fluid and electrical equipotentials are identical (*see* for example Reference 6) provided the strip is scaled so that

$$\frac{q}{p} = \frac{\log U_2}{\theta_0}$$

and

$$\frac{\partial E}{\left(\frac{\partial E}{\partial x}\right)_{AE}} = \frac{\partial \phi}{\left(\frac{\partial \phi}{\partial x}\right)_{AE}} = \frac{\partial \phi}{h/p}.$$

The intake co-ordinates are then given by

$$\frac{x}{h} = -\frac{1}{p\,U_2\left(\frac{\partial E}{\partial x}\right)_{AE}} \int_c \cos\theta\, dE$$

$$\frac{y}{h} = -\frac{1}{p\,U_2\left(\frac{\partial E}{\partial x}\right)_{AE}} \int_c \sin\theta\, dE$$

where the function $\theta = f(E)$ along CD can be obtained from measurement and $\left(\frac{\partial E}{\partial x}\right)_{AE}$ is the electrical potential gradient along the strip at AE.

The analytical solution is given in Appendix II.

For the present experiments, three intakes with contraction coefficients, $(C = h/(h+t))$, of 2/3, 4/5 and 8/9 have been calculated, the corresponding velocities, U_2, along the curved portions taking the values $\sqrt{2}$, 2 have been calculated, the corresponding velocities, U_2, along the curved portions taking the values $\sqrt{2}$, 2 and $2\sqrt{2}$ respectively (*see* Appendix II). The contractions are illustrated in Fig. 8, and the co-ordinates are intended to cover the range of lip thicknesses of practical interest, and to yield intakes on which boundary-layer control might be expected to prevent separation up to intake Mach numbers of practical importance.

4. *Experimental Details.*

The intake models were designed to be coupled to the existing Aerex centrifugal fan suction plant ancillary to the 13ft × 9ft (4m × 2·75m) wind tunnel, with a nominal flow capacity of about 5000 cu ft/min (142 cu m/min). For this reason the intake throat height was fixed at 3in (0·0762m) and the span restricted to 6in (0·152m). Although the choking mass flow for this throat area was within the nominal capacity of the pumps, a balancing problem between parallel units prevented the models being run right up to choking. It would be essential to overcome this limitation in any further experimental work.

A photograph illustrating the method of construction of the '2' intake and showing the provision for adjustment of slot width from zero to 0·050 inches (1·27mm), is given in Fig. 9. The slot width was checked with feeler gauges before installation in the rig. Twenty-two static pressure holes were provided round the surface of each intake, divided equally upstream and downstream of the slot. The airline is shown in Fig. 10 and a photograph of the front end of the apparatus is given in Fig. 11. The throat sections extends for 1ft (0·30m) in length, and 5 inches (0·127m) downstream from the slot lip, provision was made for the insertion of a thin transverse strut containing 4 pitot tubes to traverse both horizontally and vertically in order to measure the mean total pressure of the flow.

Downstream of the throat the airline diffused gently into a long length of $7\frac{3}{4}$in (0·197m) diameter tubing. The mass flow was determined at a section 9 diameters down the $7\frac{3}{4}$in diameter tubing where four pitot tubes and four static-pressure tappings were installed. The pitot tubes were adjustable and were used in a 3/4-radius position following calibration by traversing. A further 6 diameters downstream of this section, an iris-type regulating valve was installed for coarse adjustment of the flow.

The scope of the measurements undertaken is indicated in Table 3 where the Figure numbers are given in which the results may be found. In the initial run of experiments with the narrower slots, during which all the detailed static-pressure distributions were taken, the pressure of the air used for slot blowing was set at values up to 75 lb/sq in (5 atmos.) by means of an adjustable reducing valve and different inflows were obtained by setting the iris control valve at various openings. The blowing air flow was metered with a 3/4-radius type flow meter, but its indications were found to be faulty and so the flow rates were calculated from the measured pressure ratios and slot widths. A later check after an orifice-plate had been installed showed that this procedure gave results correct to within 5 per cent of directly measured values.

The later run of experiments was carried out with wider slots and the blowing flow rates were measured with the orifice-plate meter. It was found easier to ascertain critical conditions by setting the iris valve at given openings and to vary the pressure of the blowing air. However, as the extent of separation was diminished by blowing and the total-pressure recovery increased, the total mass flow increased slightly. The iris valve was not adjusted as it was not sensitive enough to allow the total inflow to be kept accurately constant. This unfortunately slightly complicates the interpretation of the measurements.

5. *Measurements.*

The following sub-sections discuss the measured characteristics of the three intakes in turn. The most readily measured characteristic is the relation between the mass flow and the static pressure far down the intake, and the theoretical work of Section 2 allows the highest static pressure achievable to be inserted as a basis for comparison. Of more importance is the value of the total pressure recovered far downstream. The accurate assessment of this required the taking and integration of some 140 readings by pitot traverse and was only attempted in a very few cases. However, using the one-dimensional approach behind the theory of Section 2 and knowing the mass-flow and the static pressure, it was possible to calculate a mean total pressure on the assumption that the velocity distribution at the throat was such that differences between $\bar{\rho}\ \bar{U}^2$ and $\overline{\rho\, U^2}$ could be neglected. It will be seen (Tables 4 and 5) that the inferred total pressure was about $1\frac{1}{2}$ per cent higher than the result obtained by pitot traverse in the case of the '$\sqrt{2}$' intake, about $\frac{1}{2}$ per cent low for the '2' intake and about $1\frac{1}{2}$ per cent low for the '$2\sqrt{2}$' intake. With a given intake there was very little difference between the errors with a without blow. It thus appears that the technique based on a single static pressure reading is suitable for making rough assessments of the effect of blowing.

Blowing increases both static pressure and total-pressure recovery, in some cases above the theoretical values possible without blowing. In order to allow the effects of blowing to be suitably assessed, therefore, an efficiency η has been used. η is defined as the ratio of the mean total-pressure recovery to that theoretically possible (including the effects of blowing), according to the theory of Section 2.

5.1. '$\sqrt{2}$' *Intake.*

Pressure distributions along this intake without blowing and with the slot sealed are shown in Fig. 12 for various mass flows. It will be seen that the largest flow achieved, 91 per cent of the ideal choking flow, was obtained without boundary-layer separation occurring, though the flow on the lip just reached sonic velocity. Compressibility effects, which were neglected in the design process, result in a modification of the pressure distribution round the curved lip, the constant-pressure region present at low mass flow giving way to a favourable pressure gradient at large flow rates. This means that for a given minimum pressure, the reduced pressures over the curved lip are not producing as large a forward-facing force component as is possible, and indicates an area in which limited improvement should be possible by a future design modification.

However, as no separation occurred, the effect of a moderate amount of blowing at the maximum intake flow (iris valve fully open) is seen in Fig. 13 to be small. The pressure distribution is virtually unaltered

although the static pressure far downstream falls slightly and this is accompanied by a 1 per cent increase in mass flow, a quantity approximately equal to that added by the blowing slot. This confirms the theoretical point made earlier that at constant mass flow, blowing raises the value of the pressure over the intake lip and decreases the forward force component†.

The mean of the static pressures measured on the upper and lower surfaces of the throat at a distance, x/h equal to 2·67 downstream from the blowing slot has been plotted as a function of the mass flow in Fig. 14, where the theoretical curve for no blowing (which is simply the static pressure associated with isentropic expansion from rest and shown in Fig. 2b) is also given. The closeness of the experimental points to the theoretical curve indicates that the losses (due to the presence of the boundary layers) are extremely small. Fig. 14 also shows two sets of observations where there was blowing through the 0·010in wide slot (0·254mm, $d/h = 0{\cdot}0033$), the iris valve remaining unaltered with and without blowing. One case comprised the observations of Fig. 13, when the blowing pressure ratio P_3/P_0 was 3·71; the other case had the pitot traverse bar in position and the blowing pressure ratio P_3/P_1 was 5·07. In the latter case, also the total resistance in the airline was slightly less so that the initial flow rate was slightly greater. In both cases the effect of blowing was to increase the total flow slightly, but only by approximately the amount injected at the slot, as can be seen in the Table 3.

The values of total-pressure recovery, both measured by pitot traverse and estimated from the measured static pressure, are given in Table 4. It can be seen that on this intake blowing effects only a small improvement. The Table also gives values of the ideal total pressure assuming mixing of the two streams without loss, following the argument of Appendix I. From these values it will be seen that the net result of blowing is about a 2 per cent reduction in efficiency in both examples. That is, the losses due to mixing exceed the potential gains in both cases.

Total-pressure profiles for the two cases where detailed measurements were taken are given in Fig. 15 for the mid-span position and are typical of the results obtained over about 80 per cent of the span of the model. The profiles confirm the absence of separation and show a flow region with enhanced total pressure despite the station being 500 slot widths downstream of the slot.

5.2. '2' *Intake.*

Pressure distributions on the '2' intake without blowing are shown in Fig. 16. At flow rates above about 73 per cent of the ideal choking flow, a patch of supersonic velocity occurred on the lip. It can be seen that separation occurred just upstream of the slot lip at all flow rates, and the downstream extent over which the static pressure rose to its final value increased with mass-flow rate (*see* broken line), suggesting an increase in length and extent of the separated-flow bubble. The separation resulted in a given mass flow being achieved at a much lower static pressure far down the intake than is given by the theory for this intake, as is seen in Fig. 17.

The effect of blowing at a pressure ratio P_3/P_0 of 4·26 through a rather narrow slot 0·005in wide (0·127mm, $d/h = 0{\cdot}0017$) is shown in Fig. 18 for a range of mass flows. At low flow rates, the pressure rise on this intake is effectively completed in a distance s/h just over 0·3. Judged by the change in extent of the region of pressure rise, therefore, it would appear that separation is prevented up to a mass-flow ratio m_1/m^* of 0·68 and that separation occurs at larger mass flows, where its prevention would require either pressure ratios above the available 5, or a wider slot. In the attached flow cases the incompressible-design velocity distribution (zero gradient on the curved lip) was again distorted with increasing flow rates to give a rising velocity on the curved surface.

Critical blowing mass flows were later established at higher intake mass flows, as is illustrated in Figs. 19 and 20 by cases with a blowing slot 0·020in wide (0·508mm, $d/h = 0{\cdot}0067$). In these examples the iris control valve and slot width were pre-set, and the pressure ratio was gradually increased. Separation was taken to be prevented when the static pressures at stations 1 and 17 were nearly equal (*see* Fig. 18),

---

†This increase in pressure over the intake lip duct blowing at constant intake mass flow is not to be confused with the change in pressure distribution near the slot seen in Fig. 13 which results from local interference effects.

though Figs. 19 and 20 show that this is not a very well defined point since the pressures at the two stations tend to approach asymptotically. The static pressures at critical conditions in the two cases are plotted in Fig. 17 for comparison. As the blowing mass flow is increased and more momentum and energy are put into the system, the mass flow into the intake m_1/m^* is seen to rise (Figs. 19, 20) at about double the rate at which the blowing mass flow increases, with a further increase in rate in the region of the critical blowing rate for the prevention of separation. Figs. 19 and 20 also show the total-pressure recovery inferred from the static pressure p_1, and the ideal value. The final collapse of the separation bubble occurs so gradually with increase of blowing that the mixing losses become important and the efficiency of total-pressure recovery reaches a rather flat maximum at a blowing rate only just over one half that required to prevent separation. Thus, for maximum efficiency, elimination of separation is not necessarily the right criterion.

Blowing to prevent separation was tried with a 0·030in wide slot (0·762mm, $d/h = 0{\cdot}010$) as well as with the narrower slots. Two cases comparing with Figs. 19 and 20 are shown in Figs. 21 and 22. Critical blowing rates are larger with the wider slots but the pressure ratios are smaller. The difference in velocity between blowing jet and intake flow is therefore less so that mixing losses are less and it will be seen that the flat peak in total-pressure recovery efficiency η now occurs roughly at the critical blowing pressure rather than well below it. Fig. 22 also shows three points obtained with decreasing blowing rate and suggests that there is a hysteresis effect on separation, but insufficient observations were taken to determine the difference in the critical quantities.

The variation of critical blowing mass-flow (measured in terms of m^*) with the intake mass flow (in the same terms) is shown in Fig. 23 and it will be seen that the influence of slot width is almost eliminated when the correlation is made in terms of momentum ratio, i.e. the ratio of the momentum in the blowing air, assuming isentropic expansion to the pressure p_1 far down the intake†, to the total momentum flux at that station. Fig. 23 covers as far as possible the higher rates of intake mass flow which are of practical interest and it should be noted that with all the observations shown, a patch of supersonic flow occurred on the lip, though this was only just the case when m_1/m^* was 0·68. There are perhaps scarcely enough observations to define closely the trend of critical momentum ratio with mass flow, but an obvious limit to extrapolation occurs near a mass-flow ratio m_1/m^* of 0·975. On theoretical grounds (Fig. 2 (c)) this inflow rate (without assistance from blowing) requires complete vacuum on the forward facing lip to balance the momentum equation and prevent separation. This represents infinite Mach number on the lip, and in practice, long before this point is reached, strong shock waves would themselves produce additional losses and provoke boundary-layer separation. Low loss operation at this flow rate would not be feasible.

The variation with mass flow of total-pressure efficiency, with and without blowing, is summarised in Fig. 24. In the cases with blowing, blowing was gradually increased at various constant iris valve settings, and the individual observations plotted in Figs. 19–22 are not shown, but the critical points at which separation is prevented are shown. The improvement in efficiency at the critical blowing rate as the slot is widened is apparent and suggests that further work with even wider slots is desirable. It is also noteworthy that owing to the small increase in total mass flow with increase of blowing rate (because of operation at constant iris valve setting) the 1 per cent increase in efficiency that was obtained at critical conditions over the no-blow result at the same valve setting actually represents a 2 per cent improvement over the no-blow result at the same mass flow.

Some Schlieren observations were attempted in order to detect the presence of shock waves but owing to faulty technique no conclusive evidence was obtained. Although the flow was locally supersonic on the lip for the highest mass-flow rates, both with and without separation, it may well be that the distribution of curvature along the streamlines—high values leading fairly abruptly into nearly zero values downstream of the slot—was such that 'peaky' pressure distributions[11] were obtained (Fig. 16 and Fig. 18 in all cases where sonic pressure ratio is exceeded) with some measure of isentropic re-compression without strong terminating shocks. In any case, such shocks as were present probably did not extend far out from

†When separation is prevented, the pressure p_1 occurs quite close to the slot. This definition of jet momentum differs from that used in Section 2, but has been chosen as a matter of convenience since p_1 was always measured, but the distribution round the curved lip was not.

the surface. Either explanation would account for the absence of any marked increase in losses.

Detailed total-pressure traverses were taken with the '2' intake for one case without blowing and for two cases with blowing rates greater than the critical so that the flow was attached. Table 5 confirms that the technique of inferring total-pressure recovery from the value of the static pressure gives answers for this intake within 0·7 per cent of the measured total-pressure recovery. Total-pressure profiles over the whole span of the intake are shown in Fig. 25 for a case with and without blowing. The improvement in profile due to the elimination of separation by blowing is marked.

In any extension of the present work, the pressure distribution on the '2' intake must be measured at flow rates approaching choking with sufficient blowing air to prevent separation. At the same time, more carefully controlled Schlieren observations are required.

5.3. '$2\sqrt{2}$' *Intake.*

Pressure distributions on the '$2\sqrt{2}$' intake without blowing are shown in Fig. 26. A patch of supersonic flow again occurred at high inflow rates and the flow separated at all inflow rates. The separation point was well upstream of the slot, and near the nose highlight. The subsequent diffusion to fill the intake took place over a distance about $2\frac{1}{2}$ times the intake height. The mean of the static pressure measured on both surfaces far down the intake is shown in Fig. 27 and it is seen that this is much lower than the optimum theoretically possible, which has been transferred from Fig. 2 (d).

The effect of blowing at a pressure ratio P_3/P_0 of 5·17 through a slot 0·010in wide (0·254mm, d/h = 0·0033) is shown in Fig. 28 for a range of intake mass flows. Judged by the extent of the region of pressure rise (which in incompressible flow extends only for 0·15h from the slot (origin)—*see* Fig. 8), separation has only been prevented at the lowest intake mass flow. The limited downstream extent of theoretical pressure rise was not appreciated at the time the measurements were made and equality of pressure between p_{15} and far downstream was assumed to signify attached flow. This may result in slightly optimistic estimations of the blowing mass-flow required to prevent separation.

Attempts to establish critical blowing mass flows at three settings of the iris control valve with a wider blowing slot (0·020in, 0·508mm, d/h = 0·0067) are illustrated in Figs. 29–31. Fig. 29 shows that prior to attachment, the separation bubble collapses slowly so that the choice of p_{17}, a station too far downstream, does not really define the critical blowing rate. At the station of p_{15} however, the pressure rises dramatically as the attachment point moves forward of this position, and it is thought that the complete elimination of separated flow would occur at a blowing rate not greatly different from that required to attach the flow at the p_{15} station.

At the two higher intake rates (Figs. 30 and 31), it was not possible to prevent separation by blowing though in both cases it will be seen that there is an initial rise in the values of p_{15} and p_{17} and an increase in total pressure efficiency, η, indicating some reduction in extent of separation, though with further increase in blowing, p_{15}, p_{17} and η decrease again. The static pressures measured without blowing and at the critical blowing rate in the case of Fig. 29 and at the maximum blowing rate in the cases of Figs. 30 and 31 are plotted in Fig. 27. It will be seen that for the case of Fig. 30, the intake throat Mach number and mass flow are close to the critical value above which separation is inevitable because the momentum balance relation would require negative pressures (i.e. less than vacuum) to maintain unseparated flow. Had the experiment illustrated in Fig. 30 been carried out at constant mass flow m_1/m^*, it is possible that separation might have been overcome, but with constant valve setting, the increase in mass flow that occurred as the separation bubble started to collapse took the flow into the regime where separation was inevitable.

It is interesting to note that both with this intake and with the '2' intake, the static pressure at the slot lip is so low at high intake mass flows that if the slot is open some small improvement is wrought by the blowing mass flow that bleeds into the intake at free stream total pressure. Indeed, Figs. 29–31 show that the total pressure efficiency reaches maxima at quite low blowing pressure ratios, in the case of Fig. 29 at a blowing mass flow only 1/3 of that required to prevent separation, which is therefore not the relevant criterion.

Critical mass flows required to prevent separation were, however, established with a variety of slot

widths, and the variation of mass-flow ratio and momentum ratio with the intake mass flow is shown in Fig. 32, though less confidence can be placed in this diagram than in the corresponding Fig. 23 for the '2' intake. At the highest intake flow at which a critical point was recorded, the flow behaviour resembled somewhat that of Fig. 30. Judged by p_{15}, unseparated flow was just achieved at the point given, but with increasing blowing pressure, the flow separated again as the total inflow increased and approached 0·7 m^* at which separation was inevitable. The reason for the high critical blowing rates at low total inflow rates is uncertain. Since no transition wires were fitted it is possible that under these conditions the flow separation that occurred was a laminar one and needed extra blowing on this account. This explanation could also account for the difference in shape of pressure distribution at mass inflow rates m_1/m^* of 0·312 and 0·438 shown in Fig. 26, but confirmation of this point requires further experimental investigation. It can be seen from Fig. 26 and is confirmed by the schlieren photographs that on this intake without blowing, separation takes place well ahead of the slot lip. A closer look should therefore be taken at critical blowing quantities to assess the hysteresis effect on separation on this intake and to determine the difference between the flow rate needed to suppress separation (to which all measurements refer) and the smaller rate at which separation redevelops.

Fig. 33 shows the variation with mass flow of the total-pressure efficiency, with and without blowing, and includes the observations of Figs. 29–31 with a slot width d/h of 0·0067 as well as one run with a slot width $d/h = 0{\cdot}0100$ and a number of critical points with wider and narrower slots. Owing to the rapid fall off in efficiency as the mass flow approaches choking (e.g. $m_1/m^* > 0{\cdot}65$) the optimum efficiency shows an even greater improvement over the no-blow condition at the same mass flow than was the case with the '2' intake (*see* Fig. 24), even though separation is not prevented. This result is of great interest, and worthy of further exploration.

However, Fig. 32 shows that although the blowing mass flows required to prevent separation on the '$2\sqrt{2}$' intake are of the order of 6 to 8 per cent of the total inflow, 3 or 4 times the corresponding mass flows required on the '2' intake, the momentum injected in 20 to 40 per cent of the total (compared with about 4 per cent for the '2' intake). The '$2\sqrt{2}$' intake must therefore be regarded as too thin for the prevention of separation by blowing to be a practical proposition.

Total-pressure profiles at the mid-span station with and without blowing are shown in Fig. 34. As the mass inflow rate was greater than 0·7 m^*, blowing was unable to prevent separation and there is no great change in profile shape in this case. Table 5 also shows that in this case blowing causes a reduction in efficiency of total-pressure recovery. Furthermore, it is interesting to note that because blowing fails to prevent separation in this example, secondary flows are present in both cases, which thin the boundary layers near the corners such that the total-pressure recoveries measured over the central two-thirds of the span (Fig. 34) are almost identical with the mean values for the whole intake (Table 5).

6. *Discussion and Conclusions.*

Two types of flow separation are distinguished in this report. The first is that which occurs in regions where the pressure gradient would be severely adverse in inviscid flow and boundary-layer control might be expected to eliminate separation and thereby increase the total-pressure recovery, and hence the mass-flow rate at a given pressure differential. Note however from the momentum equation, equation (14), that if this change in flow régime were achieved with negligible injection of momentum, the increase in downstream static pressure at the same mass-flow would be accompanied by a reduction in mean lip pressure, i.e. by an increase in the forward force developed on the lip. If on the other hand the downstream static pressure were held constant, an increase in mass-flow rate would be dependent upon an accompanying reduction in lip pressure, i.e. a greater forward lip force.

The second type of separation is that which occurs at high inflow rates in conditions where unseparated flow is impossible because it would require either a pressure less than complete vacuum on the forward-facing lip, or else one so close to vacuum that the resulting supersonic flow would introduce strong shock waves and additional losses on this count. With this type of flow, therefore, one would not expect boundary-layer control to eliminate separation, and since a reduction in lip pressure is not realisable, one would not expect a significant increase in mass flow.

These latter conclusions are also apparent from a detailed one-dimensional theoretical flow analysis which indicates in the absence of separation, or in the presence of separation of the second type, that the induction effect of blowing is small. However in view of the possibilities that boundary-layer control could effect a substantial improvement in the case of the first type of separation where at constant intake mass-flow the lip pressure might decrease appreciably, it was thought worthwhile to test three intake models with different contraction ratios.

Experiment with the thickest lipped '$\sqrt{2}$' intake (coefficient of contraction equal to 0·67) has shown that the adverse pressure gradient downstream of the intake lip was not severe enough to provoke separation up to the highest flow rate used and that the induction effect of blowing was outweighed by increased viscous losses due to the blowing.

On the middle '2' and thinnest lipped '$2\sqrt{2}$' intakes, the critical blowing mass-flow and momentum-flux ratios required to prevent separation were determined as functions of the intake mass flow. In each case, the critical blowing mass-flow ratio varied with slot width, but the momentum-flux ratio was almost independent of this parameter.

A total-pressure efficiency parameter, η, was defined as the ratio of the measured total-pressure recovery to that theoretically possible with the same blowing rate and no separation or other viscous losses, and the practical objective is to obtain the highest value of η. In the absence of blowing, this is achieved by designing to avoid separation, but with blowing, the elimination of separation is not necessarily the correct criterion. It has been found that with narrow, 0·020in wide, slots (0·51mm, $d/h = 0{\cdot}0067$), the blowing pressure ratios required to prevent separation lie between 2 and 3. The blowing velocities are then high and the ensuing mixing losses are such that the maximum values of η occur at blowing rates only 1/3 to 1/2 of the critical rates required to prevent separation. With 0·030in (0·76mm, $d/h = 0{\cdot}010$) slots on the '2' intake, the peak efficiency occurred closer to the critical blowing rate, though it was not possible to say whether the peak value was greater than with the narrower slot. However, the gain of 2 per cent in η over the unblown value at the same intake mass flow, which is the best improvement recorded so far, represents a signficant advance. The need for further tests with wider slots and lower blowing pressure ratios in order to optimise on slot width is clearly indicated. The comment should be made that as blowing is increased, the elimination of separation represents an end to the change in flow geometry. Therefore one might hope that the optimum slot width would turn out to be that for which maximum pressure recovery coincides with the elimination of separation.

Improvements in total-pressure efficiency η were unexpectedly obtained on the '$2\sqrt{2}$' intake at very high intake mass-flow rates in the range where separation was inevitable. This result is of great interest and should be explored further, by extending the tests of both the '2' and '$2\sqrt{2}$' intakes right up to choking, which was not possible with the original rig. The result obtained suggests that in these cases the separation is more extensive than it needs to be from the momentum balance point of view, being aggravated by viscous losses, and therefore susceptible to reduction by boundary-layer control. A further reason for extending the tests to choking, with both detailed pressure plotting and careful schlieren observations, is to discover at what stage shock-wave losses become significant, and the effect of boundary-layer control in this context.

The '2' intake is suitable for practical application, although a thinner lip intermediate between that of the '2' and the '$2\sqrt{2}$' intakes might be possible. The latter is too thin because although separation was prevented with blowing mass flows of the order of 6 per cent to 8 per cent of the mass flow, this represented momentum-flux ratios between 20 per cent and 40 per cent which is quite unrealistic: the corresponding values of the order of 2 per cent for mass-flow ratio and 4 per cent for momentum-flux ratio for the '2' intake are more practical.

Further gains might result from two design modifications. On the one hand, the curved lip could be modified to yield a constant pressure at the intake throat Mach number appropriate to the design mass flow rather than at zero Mach number. On the other, the impression given by the experimental work so far that patches of supersonic flow do not necessarily lead to strong shock waves and increased losses throws into question the concept that a constant-pressure lip is the ideal solution. It suggests that one might seek to improve the lip shape by attempting to achieve a definite measure of isentropic re-compression, thereby delaying to higher Mach numbers the onset of shock-wave drag. Such a refinement

in intake-lip design is not restricted either to intakes designed for operation with boundary-layer control or to intakes designed primarily for high efficiency at zero forward speed.

In addition to changes in total pressure efficiency it should be noted that the elimination of separation by blowing results also in significant improvements in the uniformity of the velocity profile at the throat.

Until the proposed further theoretical and experimental work is carried out, however, it remains difficult to make a final assessment. It is not clear whether the present improvements are sufficient to warrant the complication associated with the installation of blowing, in the face of alternative solutions for V.T.O.L. intakes based on variable-geometry lips and auxiliary inlets, but further increases in efficiency may well be possible. The advantageous use of blowing may also be possible in forward speed conditions to minimise spillage drag.

Acknowledgement.

Acknowledgement is due to Dr. A. S. Halliday, Miss S. Fermor and Mr. C. L. O'Reilly for assistance with the experimental work; to Miss E. M. Love and Miss L. M. Esson for assistance with the theoretical calculations; and to Mr. N. G. Marcus for the engineering design of the models and the rig.

NOTATION

(*see* Figure 1 and Figure 7)

a	Speed of sound
C	Coefficient of contraction, $= h/h+t$
C_p	Specific heat at constant pressure
d	Slot width
E	Electrical potential
G	Blowing parameter, defined in Section 2, equation (17)
h	Intake throat height
M	Mach number
m	Mass flow
m^*	Choking mass flow through throat height h at free-stream total pressure
m'	Choking mass flow through total height $h+t$ at free-stream total pressure
P	Total pressure
p	Static pressure
R	Gas constant
s	Distance round surface
T	Temperature
t	Lip thickness
U	Velocity
u, v	Cartesian components of velocity
x, y	Cartesian co-ordinates
γ	Ratio of specific heats
η	Total pressure efficiency, ratio of measured total pressure to ideal total pressure with blowing and no losses
θ	Angle with x-axis
ϕ, ψ	Velocity potential and stream function

Subscripts

0	(Stagnation) conditions far upstream
1	Conditions far down intake
2	Conditions on lip of intake
3	Conditions in slot
15, 17	Additional stations whose positions are indicated in Figs. 8, 16, 18, 26 and 28

Superscripts

–	Local stagnation conditions

REFERENCES

No.	Author(s)	Title, etc.
1	E. A. Fradenburgh and DeM. D. Wyatt	Theoretical performance characteristics of sharp-lip inlets at subsonic speeds. NACA Rept 1193, 1954.
2	E. J. Gabbay	Private Communication.
3	D. Küchemann and J. Weber	*Aerodynamics of Propulsion.* McGraw-Hill, 1953.
4	E. J. Gabbay	On the 'Coefficient of Contraction' for jets from two-dimensional nozzles and valve openings. Ph.D. Thesis, University of London, 1961.
5	M. S. Cahn	Solution of the incompressible free-streamline problem by electrical analogy. *J. Aero. Sci.* 29, 351, March 1962.
6	R. C. Pankhurst and D. W. Holder	*Wind Tunnel technique.* Pitman 1965 Reprint (p. 571).
7	*ibid*	(p. 27).
8	C. R. Ryan and F. F. Fleming	Some internal flow characteristics of several axisymmetrical NACA 1-series nose air inlets at zero flight speed. NACA RML54 E19a, July 1954, TIL/4295.
9	J. R. Milillo	Some internal-flow characteristics at zero flight speed of an annular supersonic inlet and an open-nose inlet with sharp and rounded lips. NACA RML54 E19, July 1954 TIL/4294.
10	J. R. Blackaby and E. C. Watson	An experimental investigation at low speeds of the effects of lip shape on the drag and pressure recovery of a nose inlet in a body of revolution. NACA Tech Note 3170. April, 1954.
11	H. H. Pearcey	The aerodynamic design of section shapes for swept wings. *Advances in Aeronautical Sciences*, Vol. 3. Pergamon Press 1961.
12	E. J. Gabbay	Improvements in or relating to fluid flow entries. Patent specification No. 1 082 202. 6th September, 1967.
13	J. Barche	Beitrag zur Gestaltung von Einläufen für Hubtriebwerke. *Z. Flugwiss* 15, (3), 98, 1967.
14	W. J. Hanbury	The performance of an air-air ejector according to a quasi-one-dimensional theory. A.R.C. 29 341, 1967.

APPENDIX I

Entropy Considerations.

The increase in entropy between stagnation conditions at station 0 far upstream and station 1 far down the intake in the absence of blowing is, per unit mass[7],

$$\log \left\{ \left(\frac{T_1}{\overline{T}_0} \right)^{C_p} \Big/ \left(\frac{p_1}{P_0} \right)^{R} \right\} .$$

When this is put $\geqslant 0$,

$$\left(\frac{T_1}{\overline{T}_0} \right)^{\frac{\gamma}{\gamma-1}} \geqslant \frac{p_1}{P_0} \quad \text{since} \quad C_p = \gamma R/\gamma - 1 .$$

The total pressure recovery, by definition, is

$$\frac{P_1}{P_0} = \frac{p_1/P_0}{(p/P)_1} = \frac{p_1/P_0}{(T_1/\overline{T}_1)^{\frac{\gamma}{\gamma-1}}}$$

But from the energy relation, $\overline{T}_0 = \overline{T}_1$, therefore

$$\frac{P_1}{P_0} \leqslant 1 .$$

Similarly, when there is blowing, the increase in entropy,

$$m_0 \log \left\{ \left(\frac{T_1}{\overline{T}_0} \right)^{C_p} \Big/ \left(\frac{p_1}{P_0} \right)^{R} \right\} + m_3 \log \left\{ \left(\frac{T_1}{\overline{T}_3} \right)^{C_p} \Big/ \left(\frac{p_1}{P_3} \right)^{R} \right\} \geqslant 0 .$$

Hence

$$\frac{T_1^{m_0 C_p} P_0^{m_0 R}}{T_0^{m_0 C_p} p_1^{m_0 R}} \geqslant \frac{\overline{T}_3^{m_3 C_p} p_1^{m_3 R}}{T_1^{m_3 C_p} P_3^{m_3 R}} .$$

Using the energy relation $\overline{T}_0 = \overline{T}_3 = \overline{T}_1$, the mass-flow relation $m_0 + m_3 = m_1$ and the stagnation relation $(P_1/p_1) = (\overline{T}_1/T_1)^{\gamma/\gamma-1}$ we obtain finally,

$$\frac{P_1}{P_0} \leqslant \left(\frac{P_3}{P_0} \right)^{m_3/m_1} .$$

APPENDIX II

Analytical Design of Optimum Intakes.

The analytical solution of the transforms illustrated in Fig. 7 may be obtained as follows:
The Schwartz-Christoffel transformation from the Q-plane to z'-plane is

$$\frac{dQ}{dz'} = K(z'-c)^{-\frac{1}{2}}(z'-d)^{-\frac{1}{2}}$$

i.e.

$$Q = \int \frac{K dz'}{\sqrt{z'^2-(c+d)z'+cd}}$$

$$= K\cosh^{-1}\frac{2z'-(c+d)}{(c-d)} + K', \qquad d > c > 0.$$

Now C, $(\log U_2, 0)$ becomes $(c, 0)$ so that $K' = \log U_2$

and D, $(\log U_2, i\theta_0)$ becomes $(d, 0)$ so that $K = -\dfrac{\theta_0}{(2n+1)\pi}$.

The transformation is thus

$$Q = -\frac{\theta_0}{(2n+1)\pi}\cosh^{-1}\frac{2z'-(c+d)}{(c-d)} + \log U_2 \tag{A.1}$$

The position in the z'-plane of the origin, B, in the Q-plane is given by

$$\cosh^{-1}\frac{2z'-(c+d)}{(c-d)} = \frac{(2n+1)\pi}{\theta_0}\log U_2$$

i.e. by

$$x'+iy' = z' = \frac{c+d}{2} + \frac{c-d}{2}\cosh\frac{\log U_2}{\theta_0/(2n+1)\pi}$$

i.e.

$$x' = \frac{c+d}{2} + \frac{c-d}{2}\cosh\frac{\log U_2}{\theta_0/(2n+1)\pi}, \quad y' = 0.$$

A further transformation, moving B in the z'-plane to the origin of a z''-plane, is effected by putting

$$z'' = z' - \frac{c+d}{2} - \frac{c-d}{2}\cosh\frac{\log U_2}{\theta_0/(2n+1)\pi} \tag{A.2}$$

so that the point C in the z''-plane has co-ordinates

$$\left(\frac{c-d}{2}\left[1-\cosh\frac{\log U_2}{\theta_0/(2n+1)\pi}\right], 0\right)$$

and D becomes

$$\left(\frac{c-d}{2}\left[-1-\cosh\frac{\log U_2}{\theta_0/(2n+1)\pi}\right],0\right).$$

The required flow, a source at B, is given by

$$F=(\phi+i\psi)=\frac{2h}{2\pi}\log z''=\frac{h}{\pi}\log(r''+i\theta''). \tag{A.3}$$

The velocity potential is

$$\phi=\frac{h}{\pi}\log r'' \tag{A.4}$$

and hence, between C and D only,

$$\frac{d\phi}{dx''}=\frac{h}{\pi x''}. \tag{A.5}$$

For any point between C and D,

$$x''=x'-\frac{c+d}{2}-\frac{c-d}{2}\cosh\frac{\log U_2}{\theta_1/(2n+1)\pi}\quad\text{from equation (A.2)},$$

and

$$\frac{2z'-(c+d)}{c-d}=\cosh i\frac{\theta}{\theta_0}(2n+1)\pi=\cos\frac{\theta}{\theta_0}(2n+1)\pi\quad\text{from equation (A.1)}.$$

Hence

$$x''=\frac{c-d}{2}\left(\cos\frac{\theta}{\theta_0}(2n+1)\pi-\cosh\frac{\log U_2}{\theta_0/(2n+1)\pi}\right). \tag{A.6}$$

The integrals in equations (18) and (19) can only be evaluated in closed form when θ_0 takes exact sub-multiple values of π. In particular, for $\theta_0=\pi$, equation (18) may be written

$$\frac{x}{h}=-\frac{1}{U_2h}\int_{x''=C}^{x''}\cos\theta\,d\phi$$

$$=-\frac{1}{U_2h}\int_{x''=C}^{x''}\left(\frac{2x''}{c-d}+\cosh\log U_2\right)\frac{h}{\pi x''}dx''\quad\text{using (A.5) and (A.6)}.$$

$$=-\frac{1}{U_2\pi}\int_{x''=C}^{x''}\left(\frac{2}{c-d}+\frac{1}{x''}\cosh\log U_2\right)dx''$$

$$= -\frac{1}{U_2\pi}\left[\frac{2x''}{c-d}+(\cosh\log U_2)\log x''\right]_{x''=\frac{c-d}{2}(1-\cosh\log U_2)}^{x''=\frac{c-d}{2}(\cos\theta-\cosh\log U_2)}$$

i.e.

$$\frac{x}{h} = -\frac{1}{U_2\pi}\left\{(\cos\theta-1)+(\cosh\log U_2)\log\frac{\cos\theta-\cosh\log U_2}{1-\cosh\log U_2}\right\}. \tag{A.7}$$

Similarly,

$$\frac{y}{h} = -\frac{1}{U_2 h}\int_{x''=C}^{x''}\sin\theta\, d\phi$$

$$= -\frac{1}{U_2\pi}\int_{x''=C}^{x''}\frac{1}{x''}\sqrt{1-\frac{4x''^2}{(c-d)^2}-\cosh^2\log U_2-\frac{4x''}{c-d}\cosh\log U_2}\,dx''$$

$$= -\frac{1}{U_2\pi(c-d)}\int_{x''=C}^{x''}\frac{-4x''^2-4x''(c-d)\cosh\log U_2+(c-d)^2(1-\cosh^2\log U_2)}{x''\sqrt{-4x''^2-4x''(c-d)\cosh\log U_2+(c-d)^2(1-\cosh^2\log U_2)}}dx''.$$

This expression can be integrated directly, and following some tedious but straightforward manipulation reduces to

$$\frac{y}{h} = -\frac{1}{U_2\pi}\left\{\sin\theta+\theta\cosh\log U_2+\sqrt{\cosh^2\log U_2-1}\left(\frac{\pi}{2}-\sin^{-1}\frac{1-\cos\theta\cosh\log U_2}{\cos\theta-\cosh\log U_2}\right)\right\}. \tag{A.8}$$

In particular, when $\theta = -\pi$, $y = t$,

$$\frac{t}{h} = -\frac{1}{U_2\pi}\left\{0-\pi\cosh\log U_2+\sqrt{\cosh^2\log U_2-1}\left(\frac{\pi}{2}-\left(-\frac{\pi}{2}\right)\right)\right.$$

$$= -\frac{1}{U_2\pi}\left\{-\frac{\pi}{2}\left(U_2+\frac{1}{U_2}\right)+\frac{\pi}{2}\left(U_2-\frac{1}{U_2}\right)\right\}$$

$$= \frac{1}{U_2^2}.$$

Hence the coefficient of contraction

$$C \equiv \frac{h}{h+t} = \frac{U_2^2}{U_2^2+1}, \tag{A.9}$$

a result that could have been simply obtained from the momentum equation (equation (14) of Section 2) assuming no blowing ($m_3 = 0$) and relating the pressures by Bernouilli's equation

$$p_0 = p_1 + \tfrac{1}{2}\rho U_1^2 = p_2 + \tfrac{1}{2}\rho U_2^2$$

since the flow has been taken to be incompressible and free from losses.

For the general case, arbitrary values of θ_0, Gabbay[12] has given a series solution in a suitable form for machine computation. The contour is

$$\frac{x}{h} = \frac{2}{U_2\pi}\left(\frac{A}{\pi}\theta_0 \sin\theta + B\cos\theta - C\right)$$

$$\frac{y}{h} = \frac{2}{U_2\pi}\left(\frac{\mathrm{A}}{\pi}\theta_0 \cos\theta - B\sin\theta\right)$$

where

$$A = \sum_{j=1}^{j=\infty} \frac{U_2^{-j\frac{\pi}{\theta_0}}}{j^2 - \left(\frac{\theta_0}{\pi}\right)^2} \sin\frac{j\pi\theta}{\theta_0}$$

$$B = \sum_{j=1}^{j=\infty} \frac{j\,U_2^{-\frac{j\pi}{\theta_0}}}{j^2 - \left(\frac{\theta_0}{\pi}\right)^2} \cos j\frac{\pi}{\theta_0}\theta$$

and

$$C = \sum_{j=1}^{j=\infty} \frac{j\,U_1^{-\frac{j\pi}{\theta_0}}}{j^2 - \left(\frac{\theta_0}{\pi}\right)^2}$$

TABLE 1

Values of the Blowing Parameter G (Section 2, equation (17)) for $d/h = 10^{-2}$.

$C = 0{\cdot}67$

P_3/P_0	2	3	4	5	7	10
m_3/m'	0·0133	0·0200	0·0267	0·0333	0·0467	0·0667
p_2/P_0	G					
0·60	0·0162	0·0276	0·0392	0·0511	0·0753	0·01126
0·528	0·0165	0·0276	0·0390	0·0507	0·0744	0·1109
·40	0·0169	0·0278	0·0389	0·0502	0·0732	0·1085
0·20	0·0180	0·0286	0·0394	0·0504	0·0727	0·1067
0	0·0242	0·0365	0·0486	0·0608	0·0850	0·1215

$C = 0{\cdot}80$

P_3/P_0	2	3	4	5	7	10
m_3/m'	0·0160	0·0240	0·0320	0·0400	0·0560	0·0800
p_2/P_0	G					
0·60	0·0177	0·0300	0·0427	0·0556	0·0820	0·1225
0·528	0·0182	0·0304	0·0430	0·0558	0·0821	0·1223
0·40	0·0191	0·0313	0·0438	0·0565	0·0825	0·01223
0·20	0·0210	0·0333	0·0458	0·0586	0·0845	0·1240
0·0	0·0290	0·0435	0·0580	0·0725	0·1016	0·1451

$C = 0{\cdot}89$

P_3/P_0	2	3	4	5	7	10
m_3/m'	0·0178	0·0267	0·0356	0·0444	0·0622	0·0889
p_2/P_0	G					
0·60	0·0186	0·0316	0·0449	0·0585	0·0863	0·1289
0·528	0·0193	0·0323	0·0456	0·0593	0·0871	0·1298
0·40	0·0205	0·0337	0·0471	0·0609	0·0888	0·1316
0·20	0·0229	0·0366	0·0504	0·0645	0·0929	0·1364
0	0·0323	0·0489	0·0651	0·0814	0·1140	0·1628

$C = 1{\cdot}0$

P_3/P_0	2	3	4	5	7	10
m_3/m'	0·02	0·03	0·04	0·05	0·07	0·10
p_2/P_0	G					
0·60	0·0195	0·0330	0·0469	0·0611	0·0902	0·1348
0·528	0·0204	0·0340	0·0481	0·0624	0·0917	0·1367
0·40	0·0220	0·0360	0·0504	0·0650	0·0949	0·1406
0·20	0·0252	0·0399	0·550	0·703	·1014	0·1488
0·0	0·0363	0·0544	0·0725	0·0907	0·1269	0·1813

TABLE 2

Co-ordinates of Three Intake Shapes.

U_2/U_1	$\sqrt{2}$		2		$2\sqrt{2}$	
Coefficient of Contraction	0·67		0·80		0·89	
θ deg	x/h	y/h	x/h	y/h	x/h	y/h
0	0	0	0	0	0	0
5	−0·0136	0·0008	−0·0024	0·0001	−0·0007	0
10	−0·0497	0·0057	−0·0093	0·0011	−0·0028	0·0003
15	−0·0987	0·0166	−0·0199	0·0035	−0·0062	0·0011
20	−0·1510	0·0331	−0·0333	0·0077	−0·0105	0·0025
25	−0·2017	0·0541	−0·0483	0·0139	−0·0157	0·0046
30	−0·2479	0·0781	−0·0639	0·0220	−0·0214	0·0076
35	−0·2887	0·1041	−0·0793	0·0319	−0·0272	0·0113
40	−0·3241	0·1312	−0·0939	0·0430	−0·0331	0·0158
45	−0·3543	0·1588	−0·1072	0·0553	−0·0388	0·0210
50	−0·3796	0·1864	−0·1192	0·0684	−0·0441	0·0268
55	−0·4005	0·2137	−0·1296	0·0819	−0·0488	0·0330
60	−0·4175	0·2402	−0·1384	0·0957	−0·0530	0·0395
65	−0·4308	0·2658	−1·455	0·1094	−0·565	0·0463
70	−0·4410	0·2903	−0·1511	0·1229	−0·0593	0·0531
75	−0·4483	0·3136	−0·1553	0·1360	−0·0615	0·0599
80	−0·5432	0·3355	−0·1581	0·1486	−0·0629	0·0665
85	−0·4559	0·3559	−0·1597	0·1607	−0·0638	0·0730
90	−0·4567	0·3749	−0·1602	0·1719	−0·0641	0·0792
95	−0·4560	0·3923	−0·1597	0·1824	−0·0638	0·0850
100	−0·4539	0·4082	−·1584	0·1921	−0·0631	0·0904
105	−0·4508	0·4224	−0·1565	0·2209	−0·0620	0·0954
110	−0·4467	0·4352	−0·1540	0·2088	−0·0606	0·0999
115	−0·4420	0·4465	−0·1511	0·2158	−0·0589	0·1040
120	−0·4370	0·4562	−0·1479	0·2219	−0·0570	0·1076
125	−0·4317	0·4646	−0·1446	0·2272	−0·0551	0·1106
130	−0·4263	0·4715	−0·1412	0·2316	−0·0531	0·1133
135	−0·4211	0·4773	−0·1378	0·2352	−0·0511	0·1154
140	−0·4161	0·4819	−0·1347	0·2382	−0·0492	0·1172
145	−0·4114	0·4855	−0·1317	0·2405	−0·0474	0·1186
150	−0·4073	0·4881	−0·1290	0·2422	−0·0458	0·1196
155	−0·4037	0·4900	−0·1267	0·2434	−0·0444	0·1203
160	−0·4008	0·4912	−0·1249	0·2441	−0·0433	0·1208
165	−0·3988	0·4919	−0·1236	0·2446	−0·0425	0·1210
170	−0·3975	0·4921	−0·1227	0·2447	−0·0420	0·1211
175	−0·3970	0·4922	−0·1225	0·2448	−0·0418	0·1212

TABLE 3

Summary of Measurements, with Figure Numbers.

		Intake	
	'$\sqrt{2}$'	'2'	'$2\sqrt{2}$'
Initial experiments with narrow slots (d/h = 0·001, 0·0017, 0·003)			
Static-pressure distributions (slot sealed)	12	16	26
Variation of mass flow with pressure drop	14		
Static-pressure distributions with constant blowing mass flow, varied iris-valve settings	13	18	28
Later experiments with wide slots (d/h = 0·0067, 0·0100)			
Variation of mass flow with pressure drop (slot sealed)		17	27
Effect of blowing-pressure ratio on intake characteristics (at fixed iris-valve settings)		19 20 21 22	29 30 31
Variation of critical blowing mass-flow and momentum ratios and of total-pressure efficiency with total mass flow		23 24	32 33
Total-pressure traverses	15 Table 4	25 Table 5	34 Table 5

TABLE 4

Details of some '$\sqrt{2}$' Intake Cases given in Fig. 14, Showing Effect of Slot Blowing on Total-Pressure Recovery, Measured and Inferred, at High Intake Mass Flows.

Symbol in Fig. 14	Mass-flow ratios			Blowing-Pressure ratio, P_3/P_0	Slot width d/h	Static pressure p_1/P_0	Total-pressure recovery P_1/P_0			Total-pressure recovery / Ideal pressure recovery, η		Comment
	m_1/m^*	m_3/m^*	m_3/m_1				Inferred from static pressure	From pitot traverse	Ideal value	Inferred	Measured	
*	0·910	0	0	—	—	0·725	1·000		1·000	1·000		Same control valve settings
o	0·919	0·0124	0·0135	3·71	0·0033	0·707	0·995		1·018	0·977		
+	0·917	0	0	—	—	0·700	0·990	0·976	1·000	0·990	0·976	Same control valve settings in presence of traverse gear
□	0·934	0·0170	0·0182	5·07	0·0033	0·696	0·999	0·984	1·030	0·970	0·956	

TABLE 5

Details of Pitot-Traverse Cases on '2' and '2√2' Intakes, Showing Comparison between Measured and Inferred Total-Pressure Recovery at High Intake Mass Flows with and without Slot Blowing.

Intake	Mass-flow ratios			Blowing-pressure ratio P_3/P_0	Slot width d/h	Static pressure p_1/P_0	Total-pressure recovery, P_1/P_0			Total-pressure recovery / Ideal pressure recovery, η		Comment
	m_1/m^*	m_3/m^*	m_3/m_1				Inferred from static pressure	From pitot traverse	Ideal value	Inferred	Measured	
2	0·828	0	0	—	—	0·705	0·939	0·943	1·000	0·939	0·943	Same control valve settings
	0·865	0·0275	0·0319	5·15	0·0033	0·708	0·963	0·970	1·054	0·914	0·920	
	0·850	0·0227	0·0227	3·04	0·0067	0·736	0·971	0·977	1·028	0·944	0·950	Blowing greater than critical quantity
2√2	0·708	0	0	—	—	0·708	0·877	0·894	1·000	0·877	0·894	
	0·755	0·0174	0·0231	5·23	0·0033	0·707	0·901	0·911	1·039	0·867	0·877	Separation inevitable

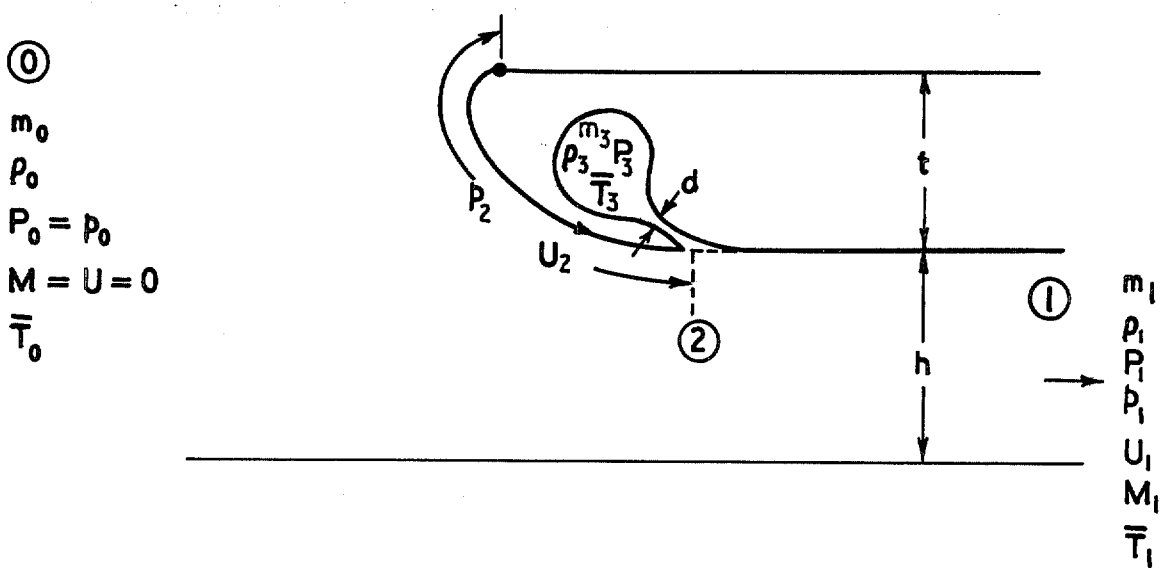

FIG. 1. Flow quantities associated with optimum intake.

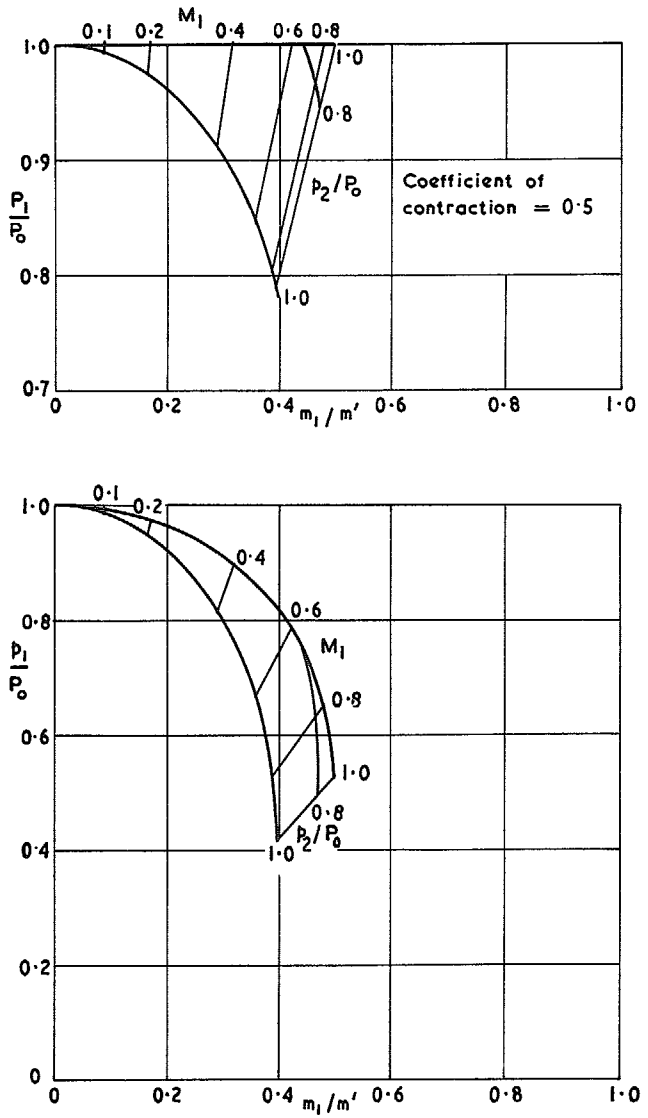

FIG. 2a. Theoretical performance of intake with coefficient of contraction = 0·5.

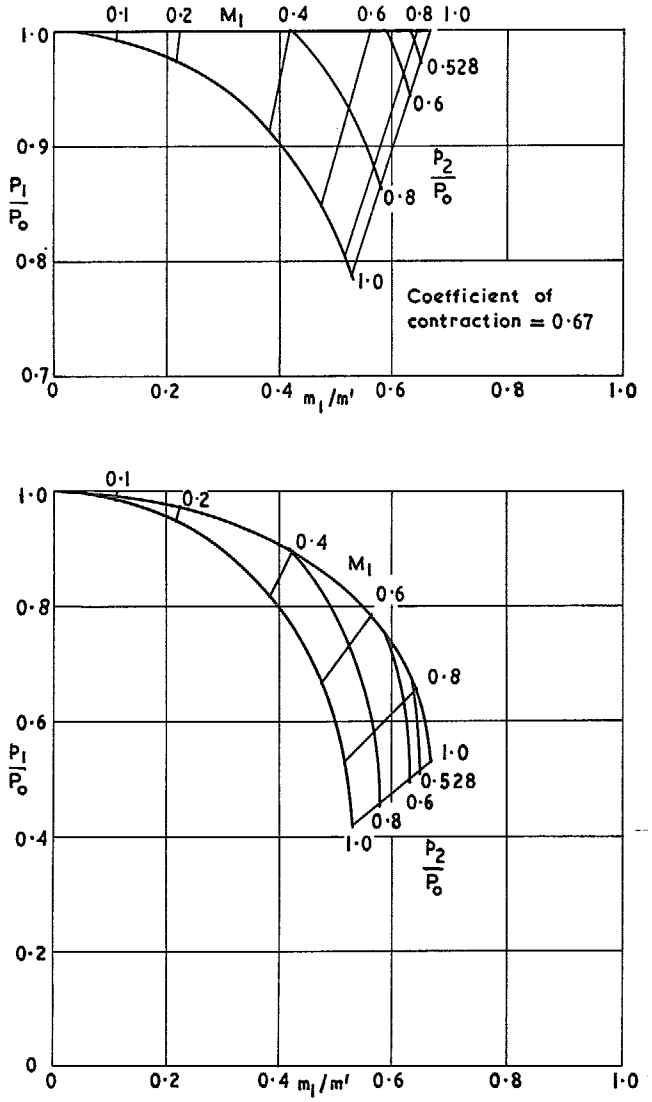

FIG. 2b. Theoretical performance of intake with coefficient of contraction = 0·67.

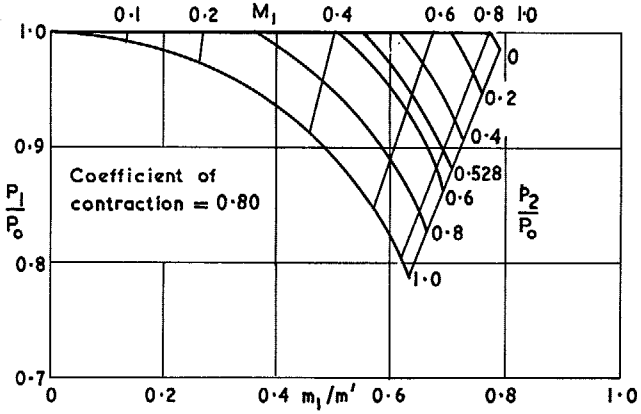

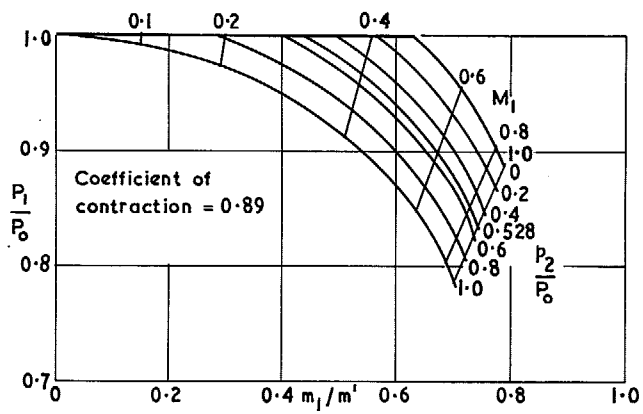

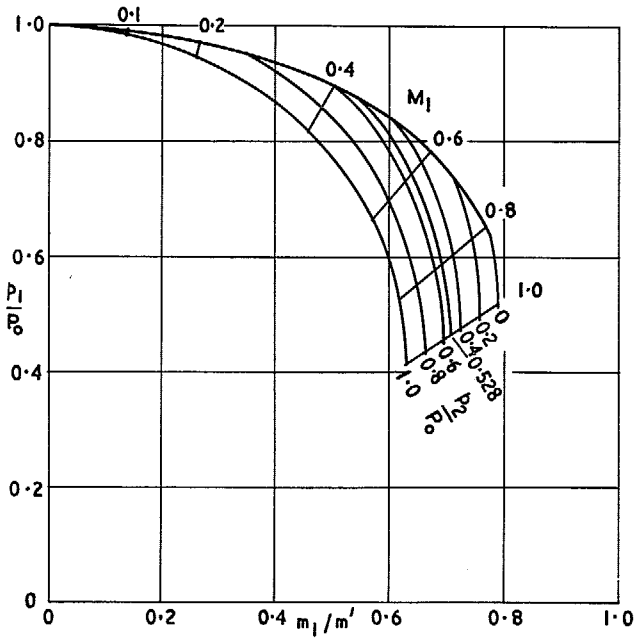

FIG. 2c. Theoretical performance of intake with coefficient of contraction = 0·80.

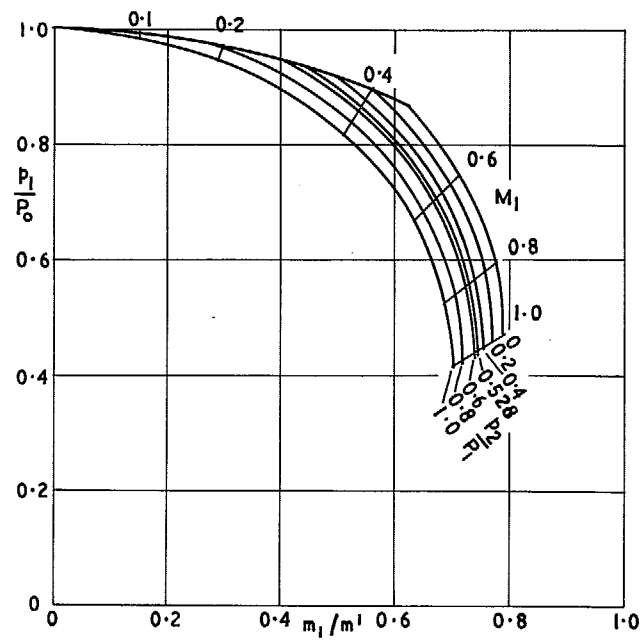

FIG. 2d. Theoretical performance of intake with coefficient of contraction = 0·89.

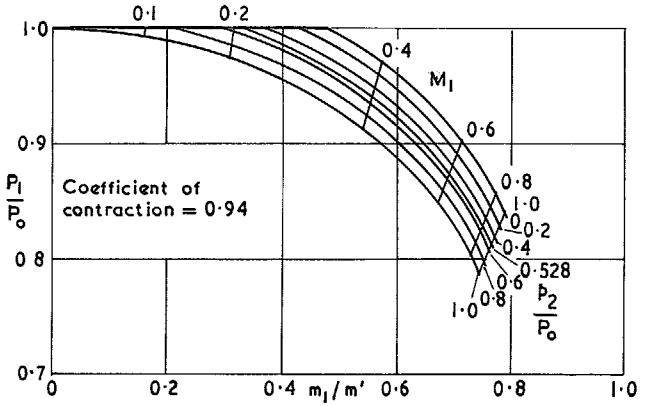

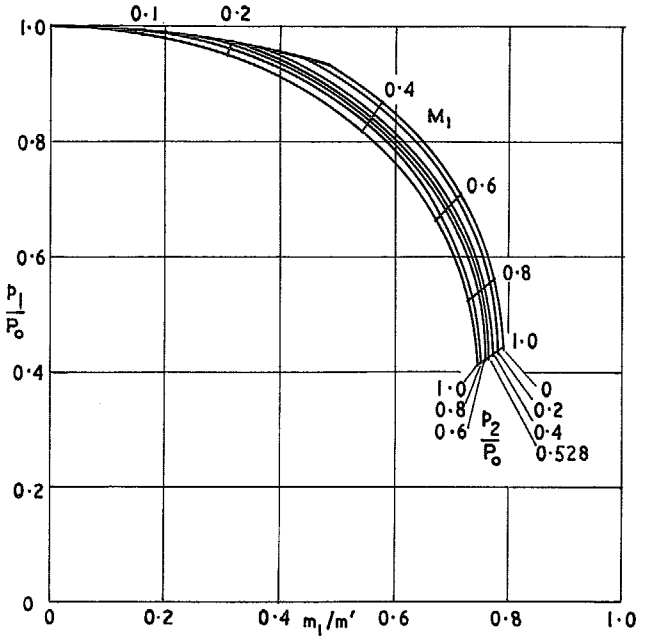

FIG. 2e. Theoretical performance of intake with coefficient of contraction = 0·94.

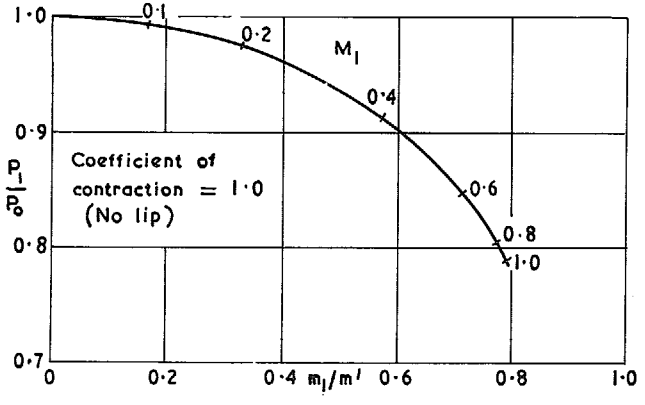

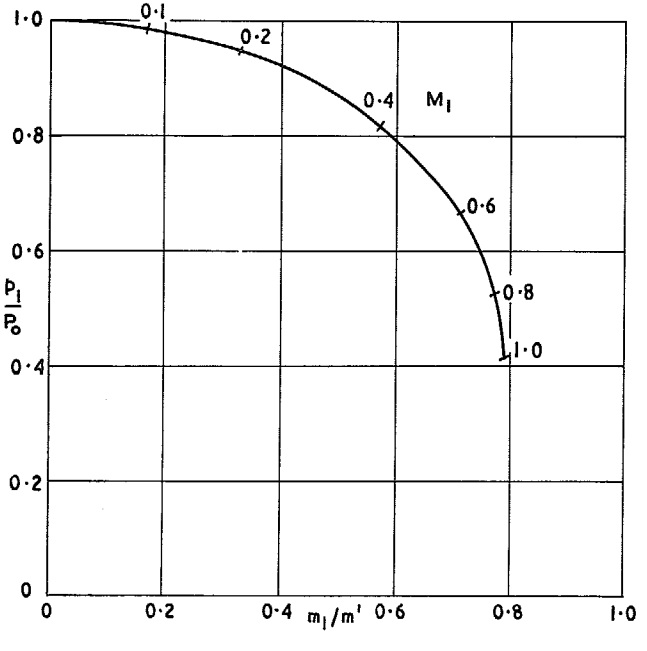

FIG. 2f. Theoretical performance of intake with coefficient of contraction = 1·0.

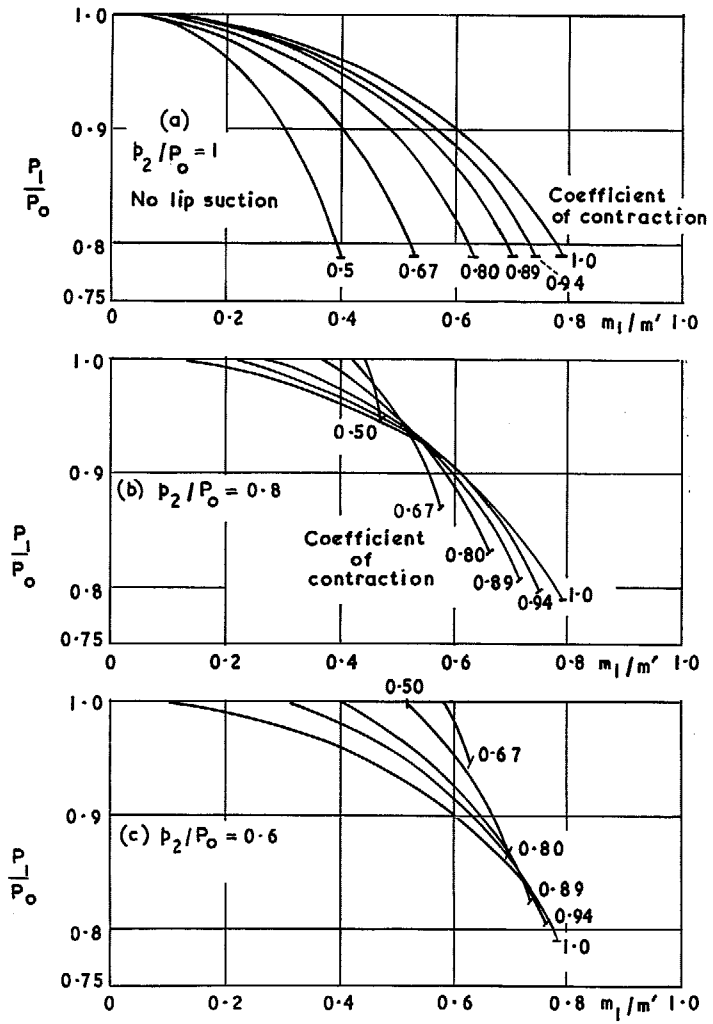

FIG. 3 (a to c). Variation of inlet total pressure with mass flow ratio and coefficient of contraction for lip pressures $p_2/P_0 = 1, 0{\cdot}8, 0{\cdot}6$.

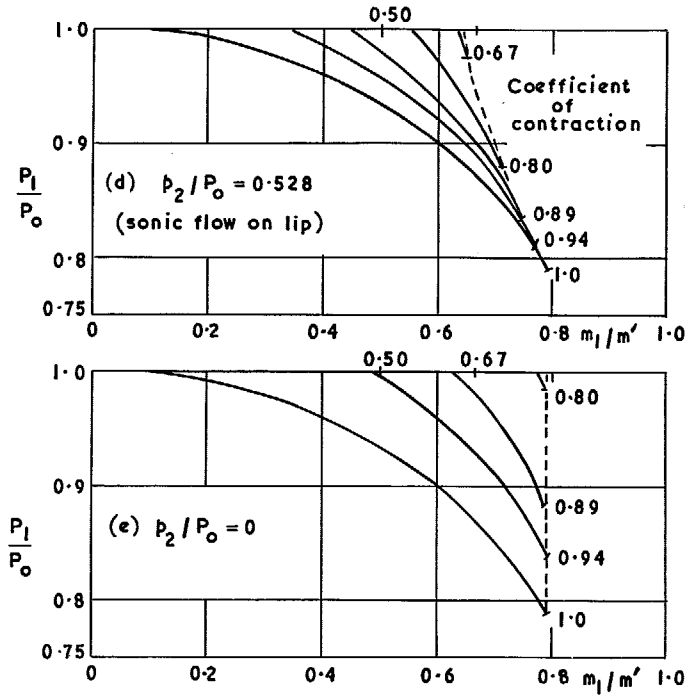

FIG. 3 (d & e). Variation of inlet total pressure with mass flow ratio and coefficient of contraction for lip pressures $p_2/P_0 = 0{\cdot}528$ and 0.

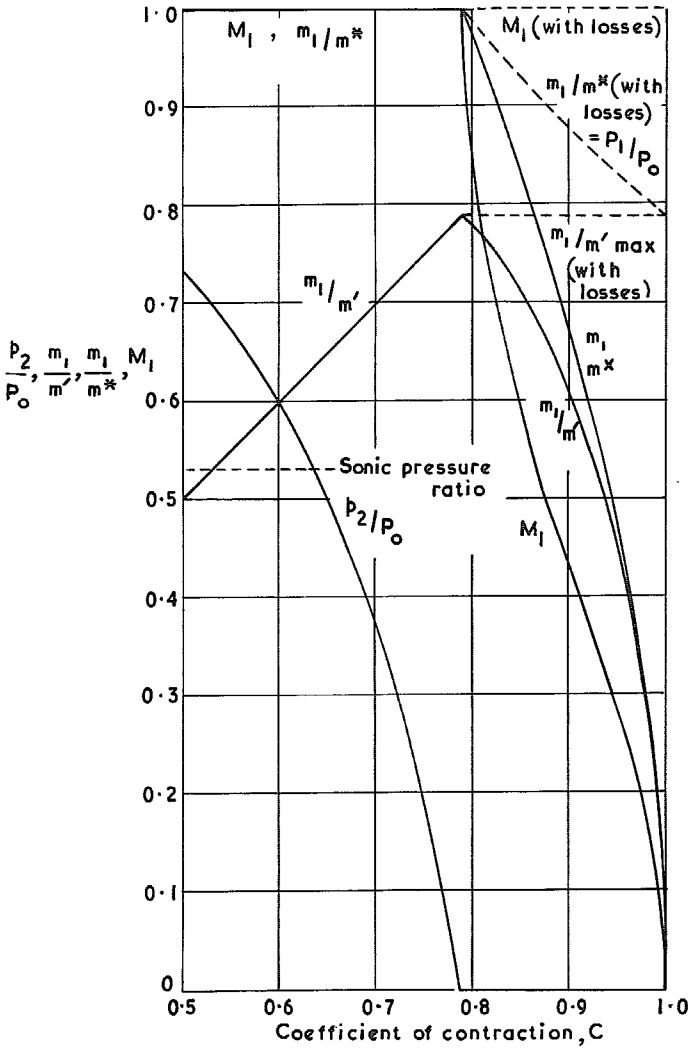

FIG. 4. Maximum flow rate, and maximum flow rate for no losses, together with mean lip pressure, intake Mach number and total pressure recovery as functions of coefficient of contraction.

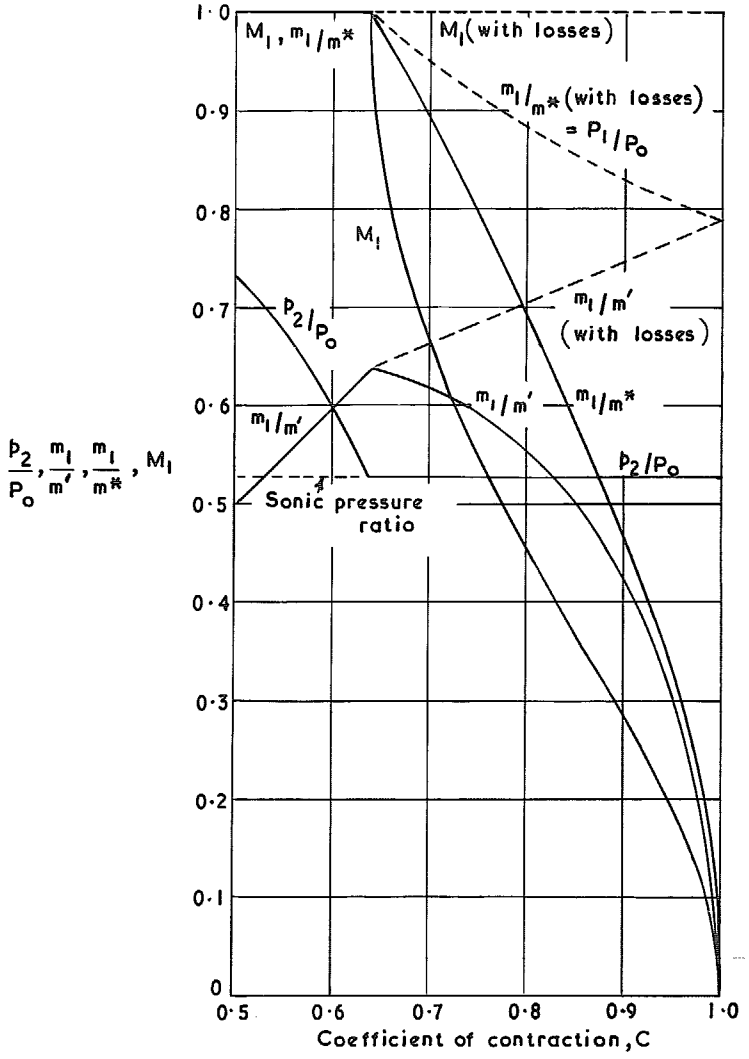

FIG. 5. Maximum flow rate, and maximum flow rate for no losses, together with mean lip pressure, intake Mach number and total pressure recovery as functions of coefficient of contraction, with the additional restriction that the lip pressure ratio is not less than 0·528, the sonic value.

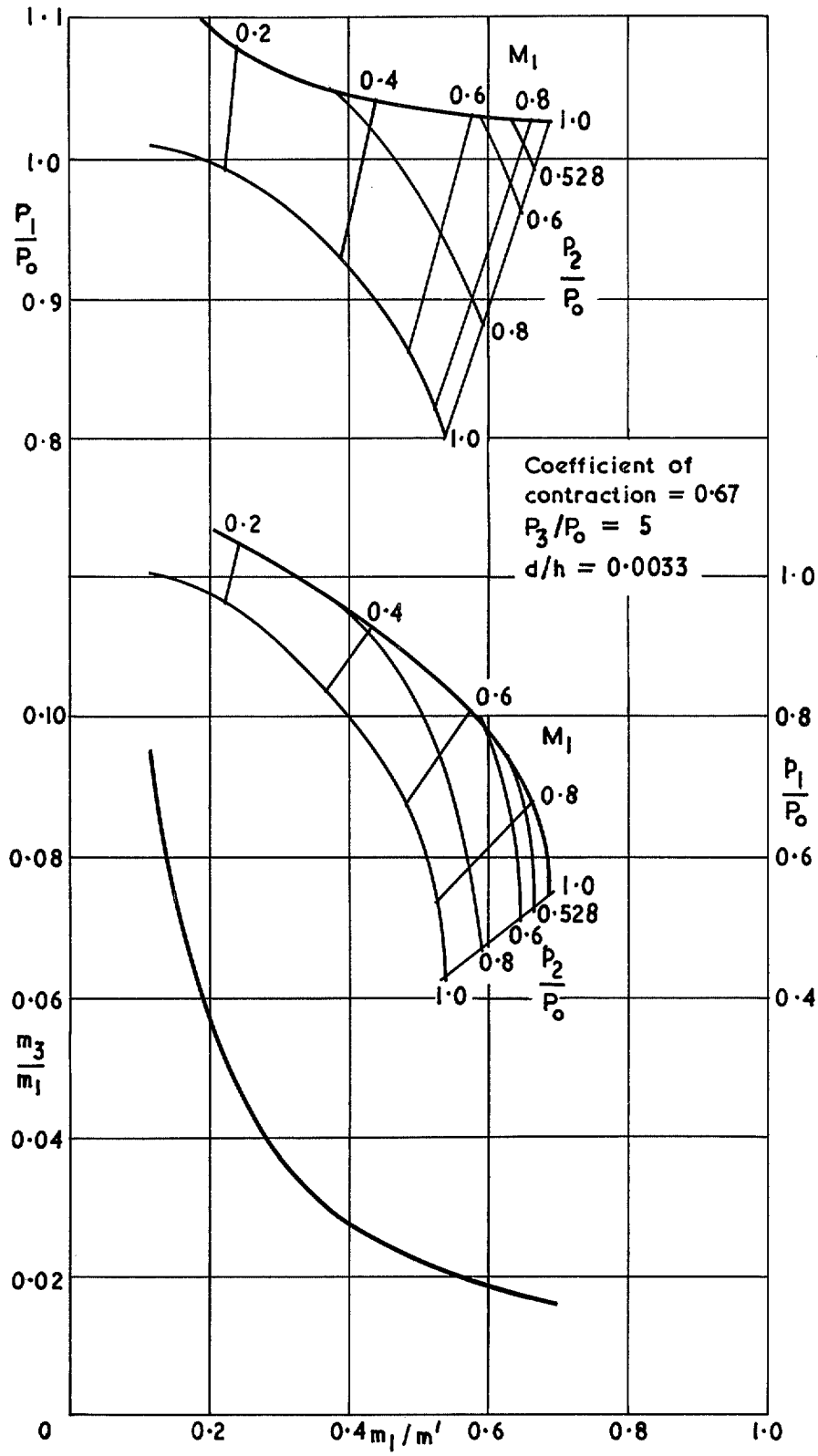

FIG. 6a. Theoretical performance of intake with coefficient of contraction = 0·67 with blowing. $P_3/P_0 = 5$, $d/h = 0{\cdot}0033$ (Compare with Fig. 2 b).

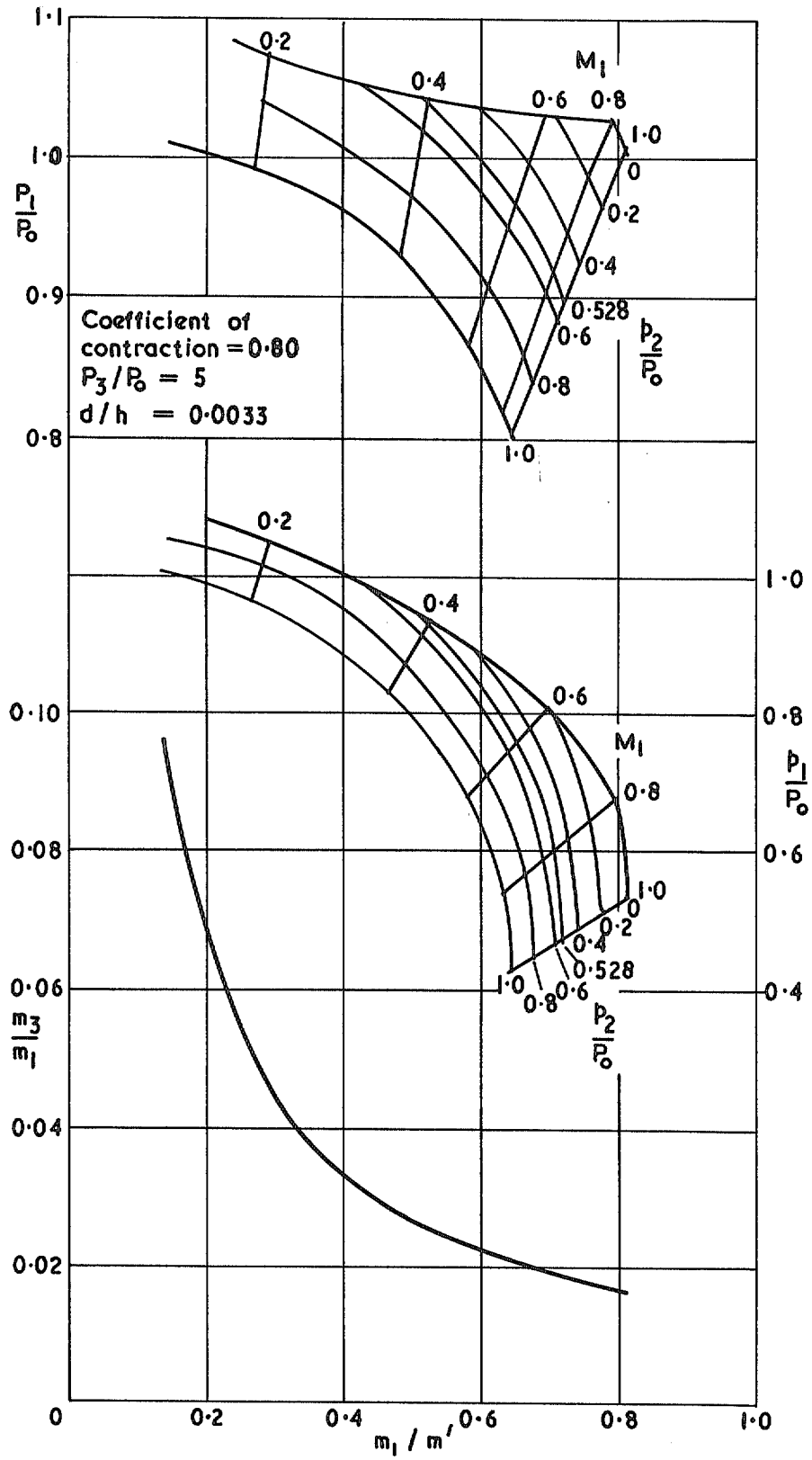

FIG. 6b. Theoretical performance of intake with coefficient of contraction = 0·80 with blowing. $P_3/P_0 = 5$, $d/h = 0{\cdot}0033$ (Compare with Fig. 2 c).

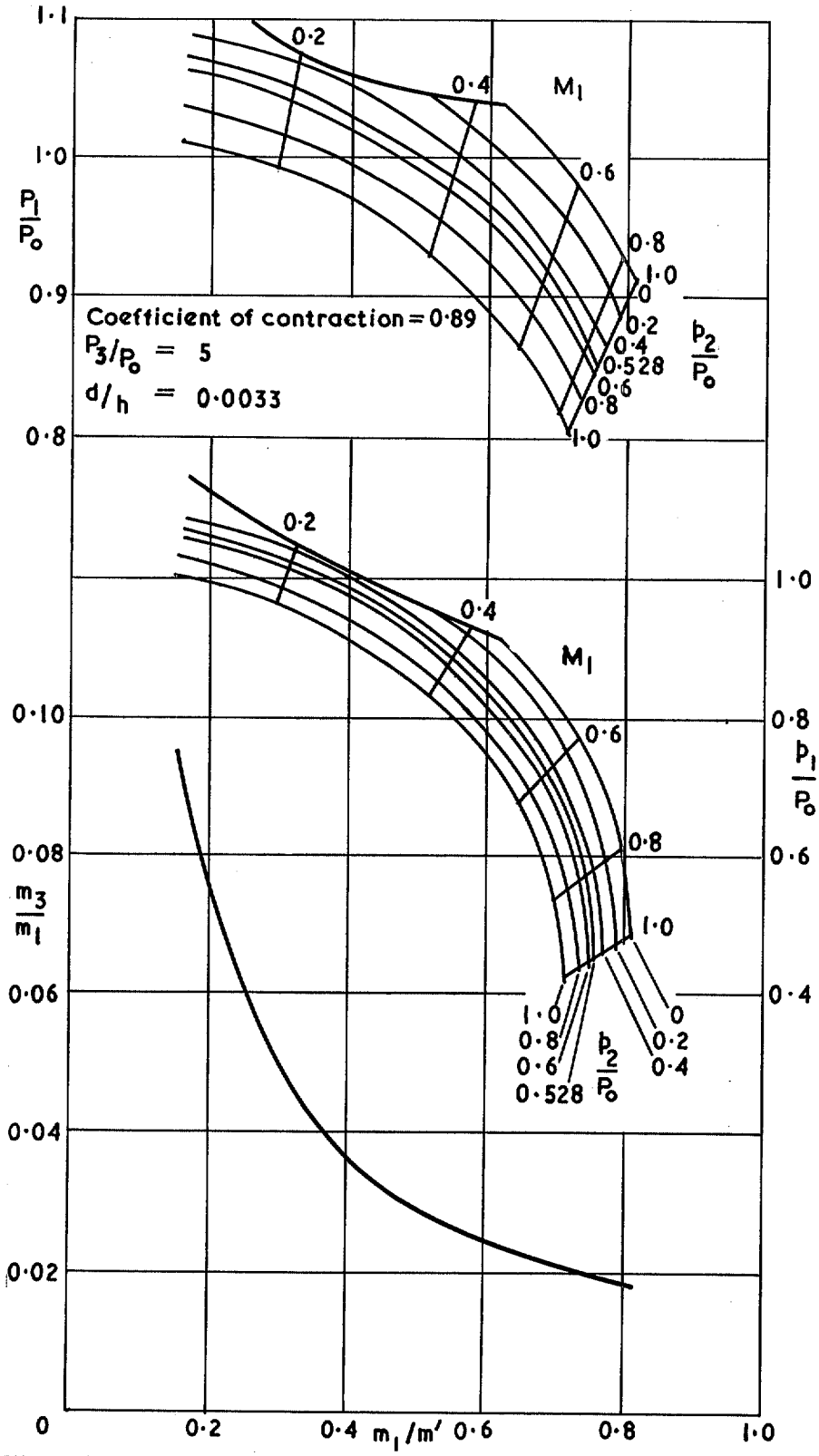

FIG. 6c. Theoretical performance of intake with coefficient of contraction = 0·89 with blowing. $P_3/P_0 = 5$, $d/h = 0{\cdot}0033$ (Compare with Fig. 2d).

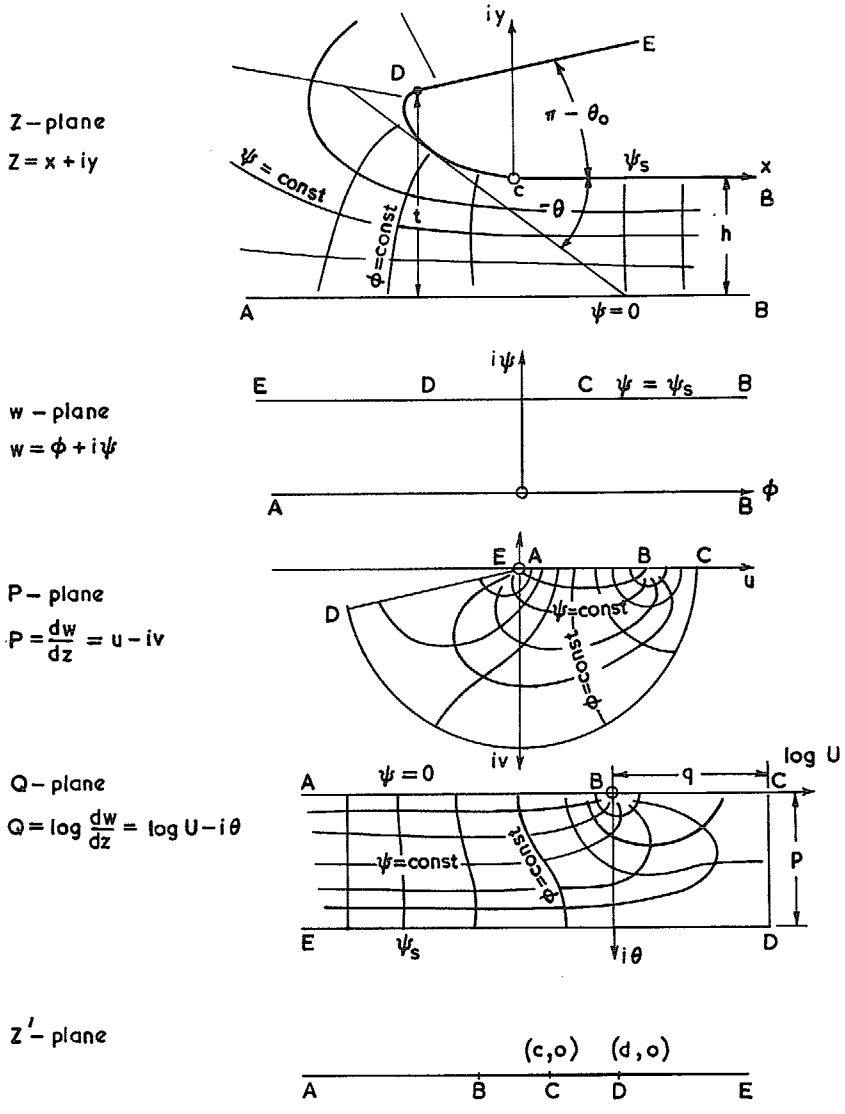

FIG. 7. Conformal maps of the intake boundaries used in the design of 'optimum' intakes.

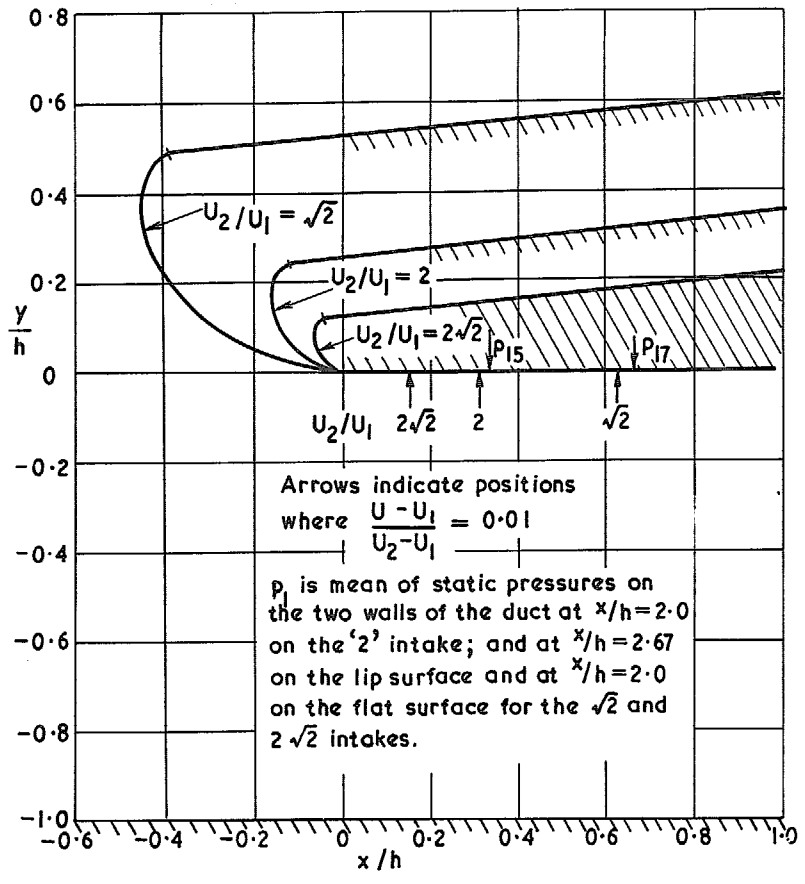

FIG. 8. Sections of three two-dimensional intake shapes, showing theoretical position of limits to pressure recovery, and positions of certain static pressure tappings.

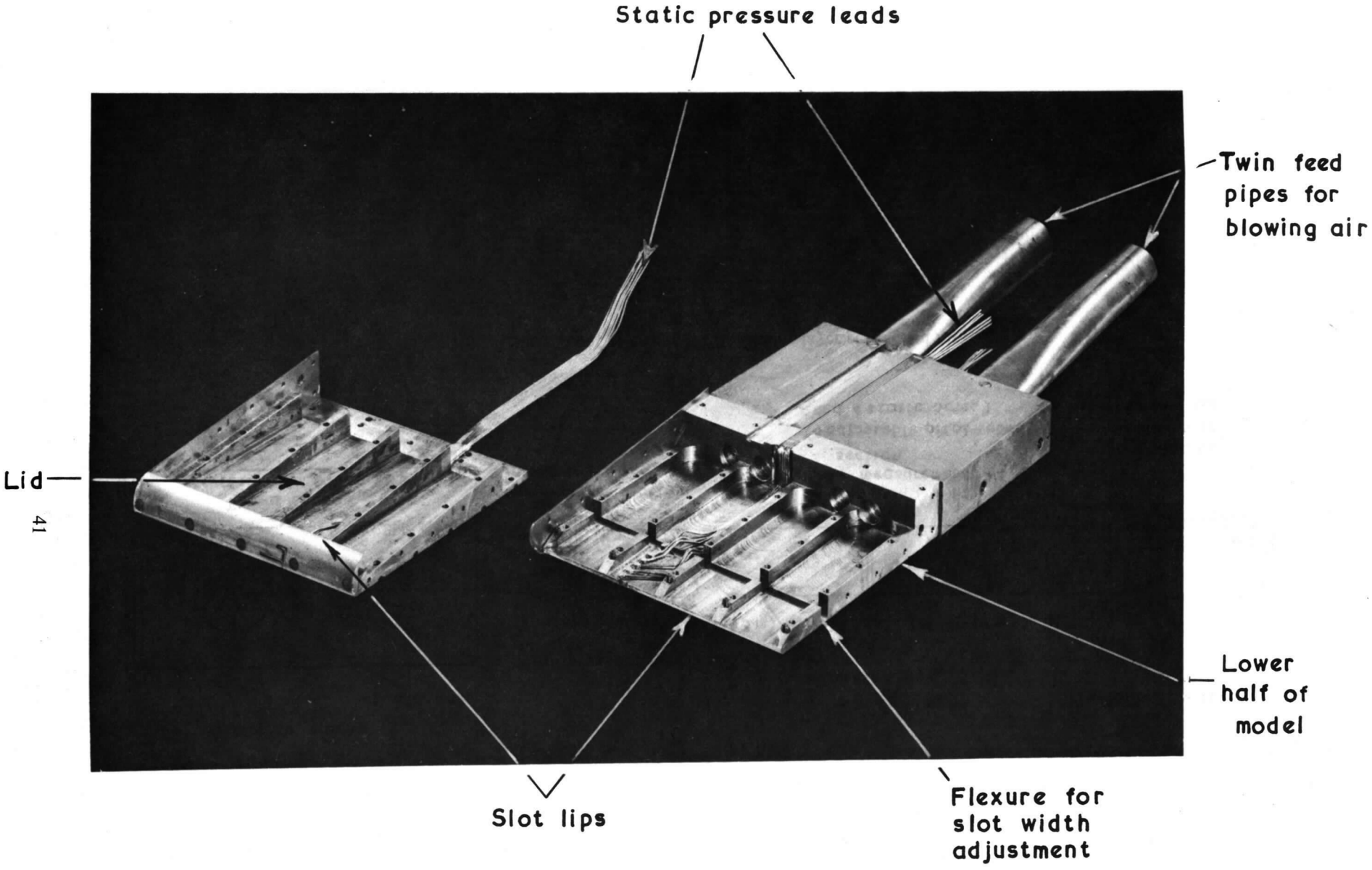

FIG. 9. Exploded view of '2' intake.

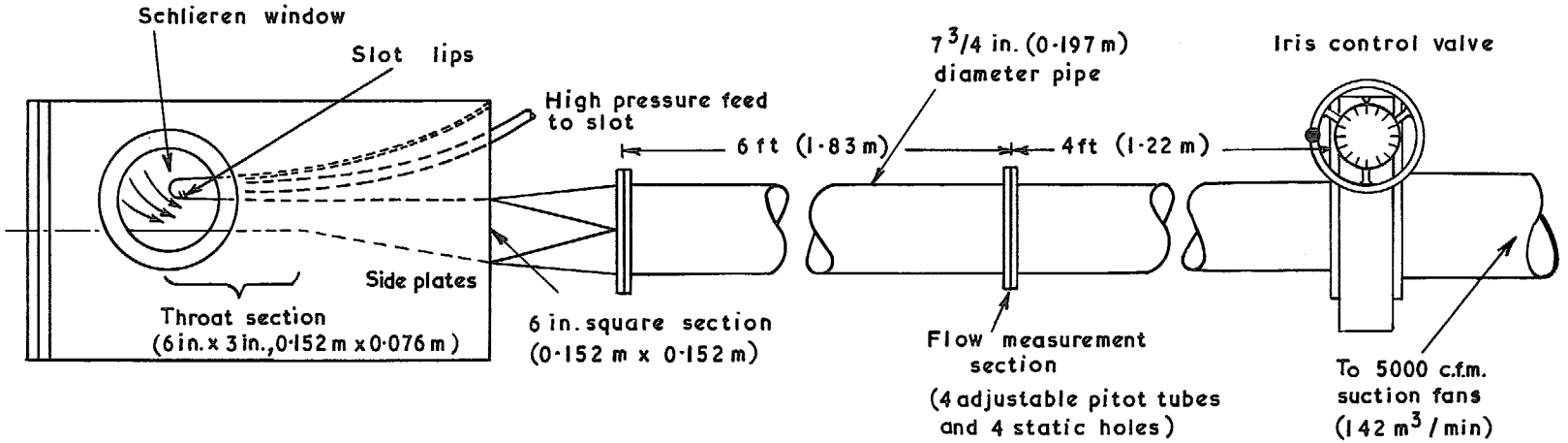

FIG. 10. Arrangement of airline for boundary-layer controlled intakes.

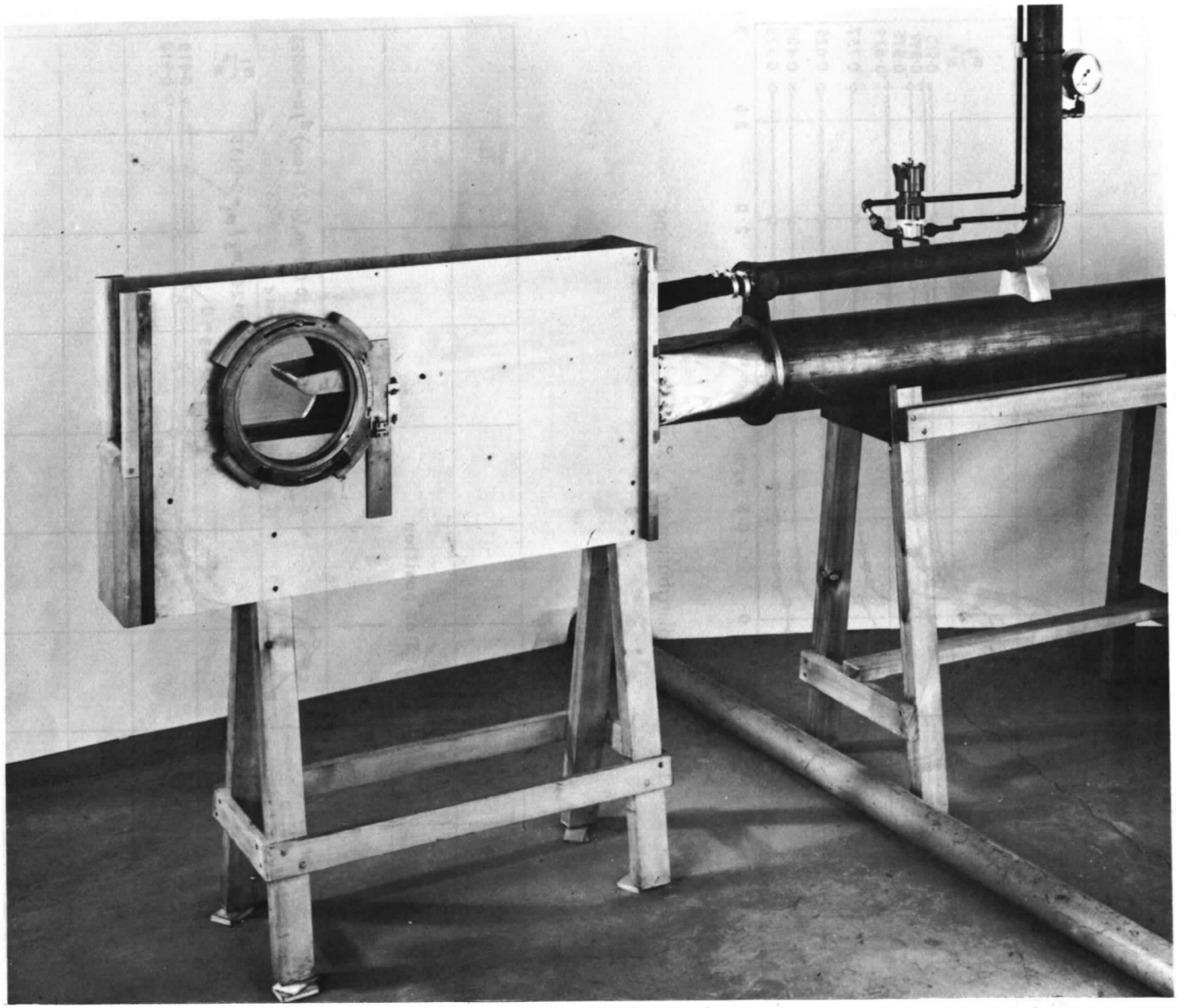

FIG. 11. Front end of boundary-layer controlled intake rig.

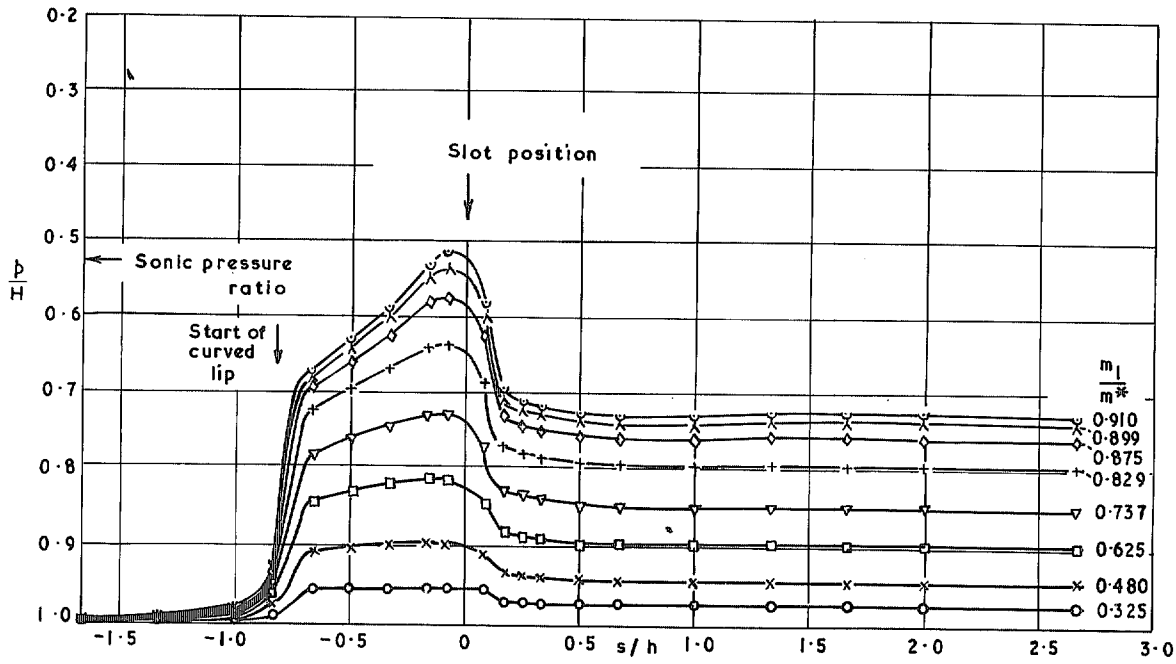

FIG. 12. Pressure distribution on '$\sqrt{2}$' intake without blowing.

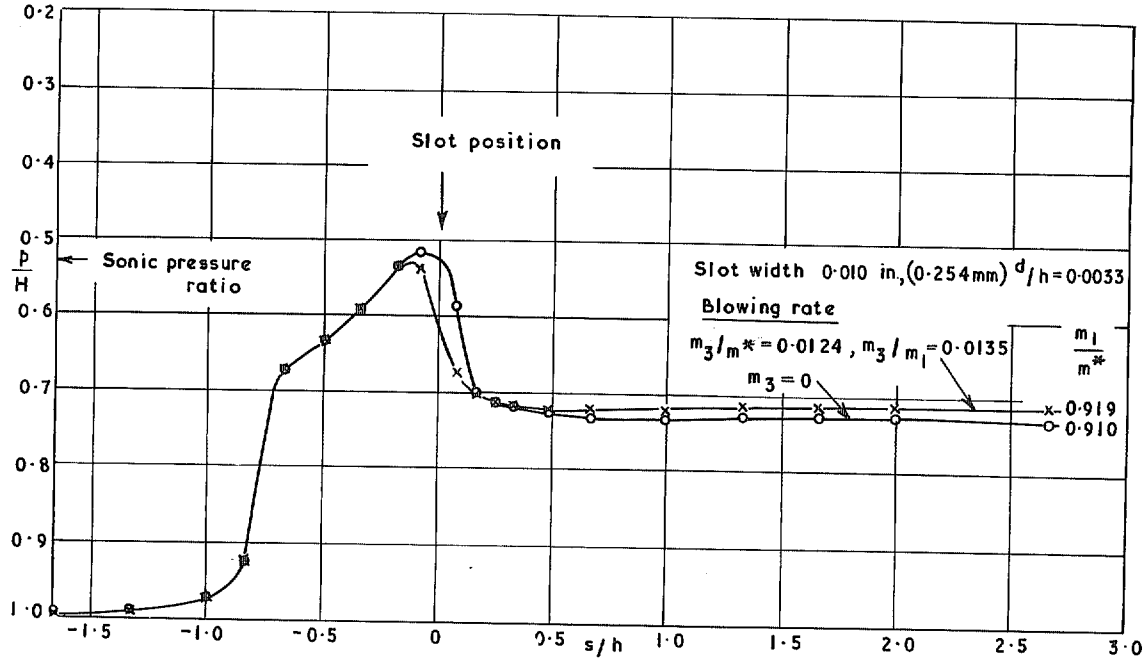

FIG. 13. Effect of blowing on pressure distribution on $\sqrt{2}$ intake at a large mass flow rate.

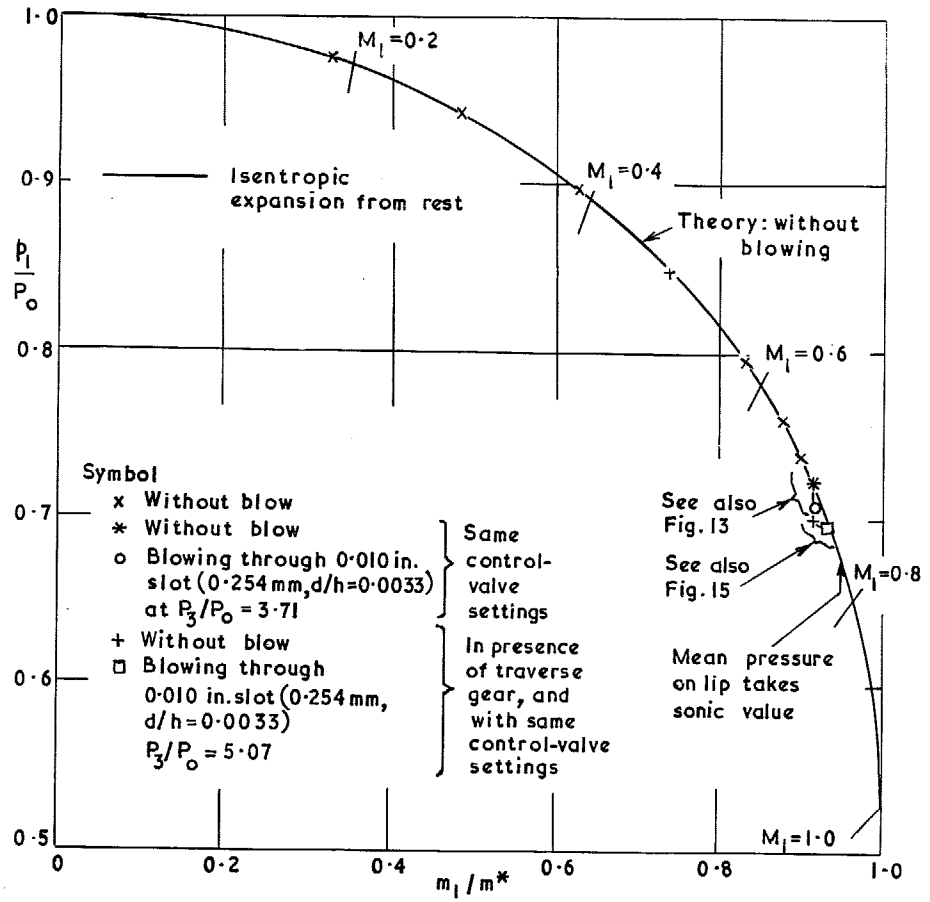

FIG. 14. Variation with mass flow of static pressure far down '$\sqrt{2}$' intake with and without blowing.

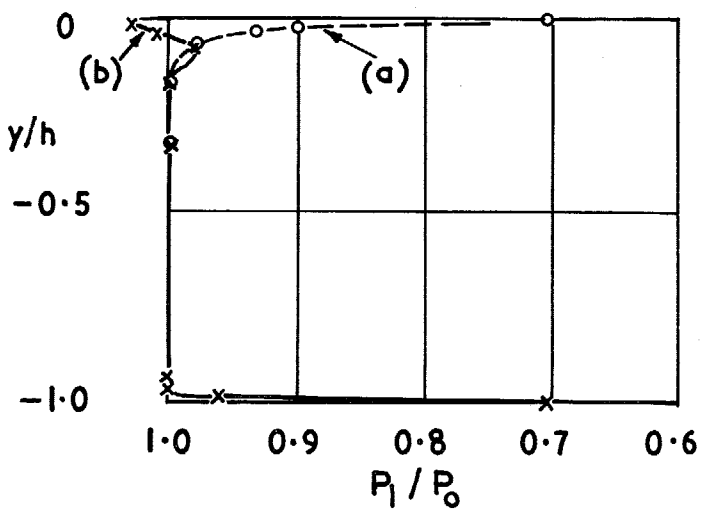

FIG. 15. Total pressure profiles in '$\sqrt{2}$' intake at mid-span station, 1·67h downstream of slot lip
(a) without blowing, $m_1/m^* = 0{\cdot}917$ Mean $P_1/P_0 = 0{\cdot}993$ (mid-span)
(b) with blowing, $m_1/m^* = 0{\cdot}934$, $m_3/m^* = 0{\cdot}0170$, $m_3/m_1 = 0{\cdot}0182$ $P_3/P_0 = 5{\cdot}07$, $d/h = 0{\cdot}0033$, Mean $P_1/P_0 = 0{\cdot}997$ (mid-span).

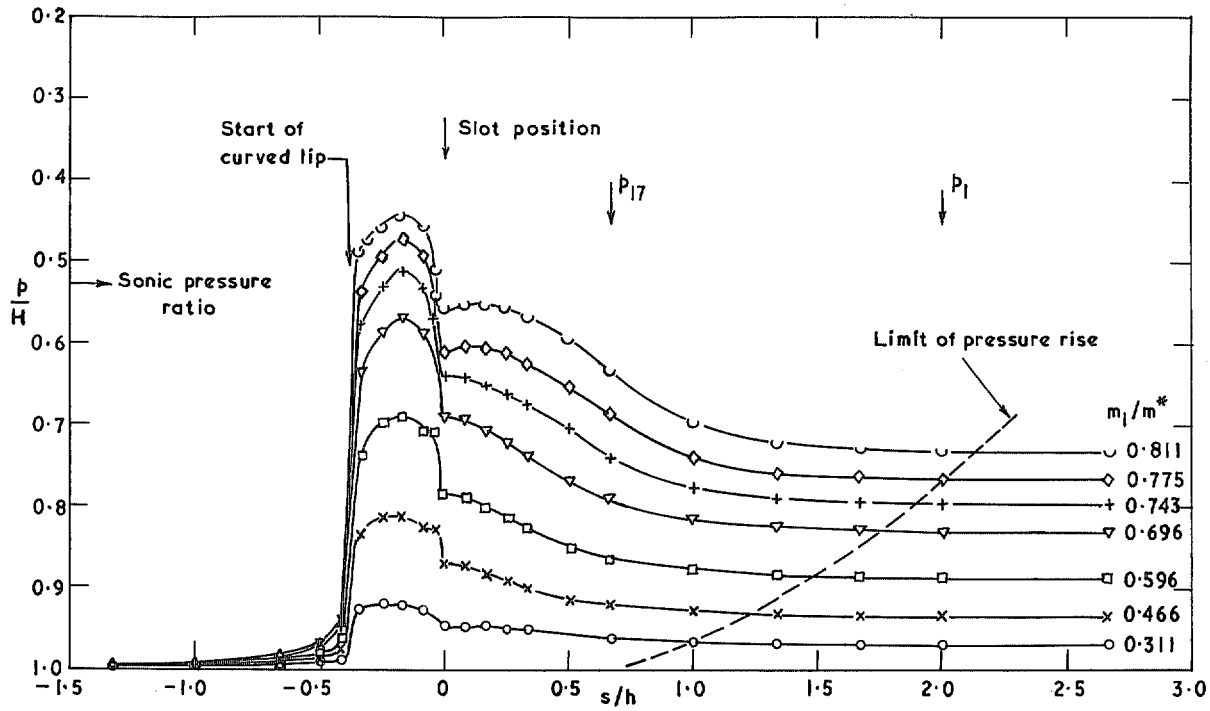

FIG. 16. Pressure distribution on '2' intake without blowing.

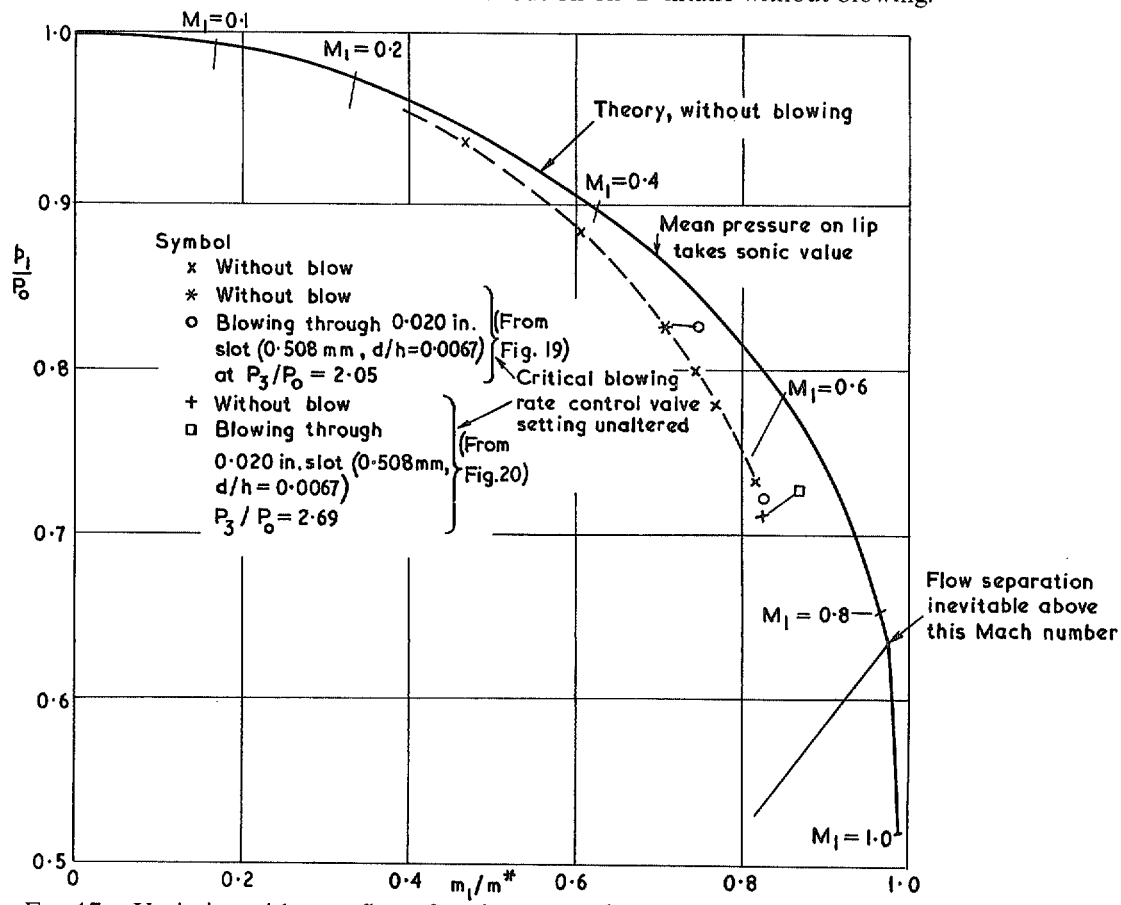

FIG. 17. Variation with mass flow of static pressure far down '2' intake, with and without blowing.

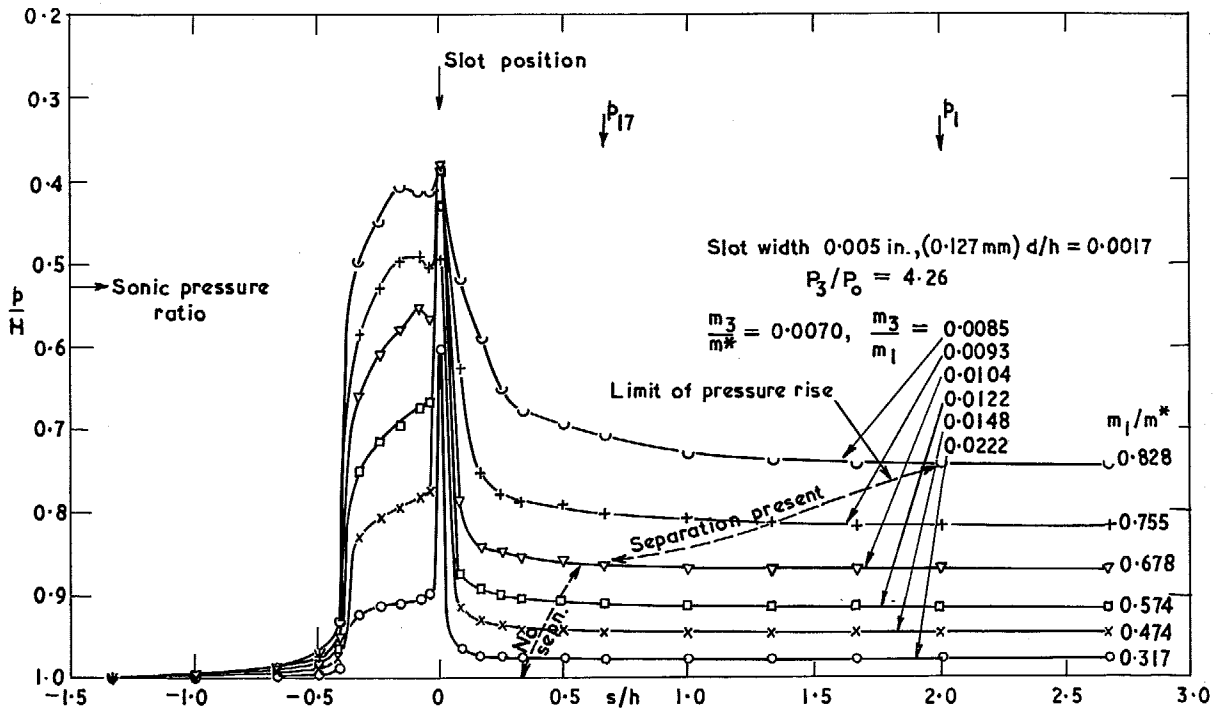

FIG. 18. Effect of a constant blowing rate on pressure distribution on '2' intake.

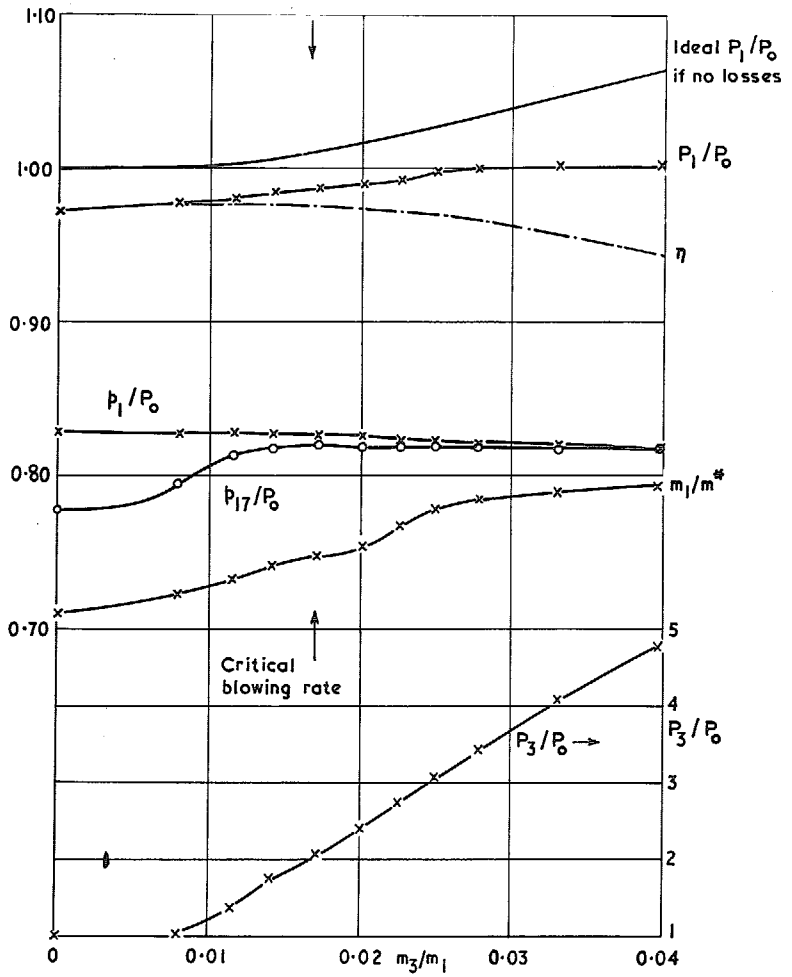

FIG. 19. Variation with blowing rate through a 0·020 in slot (0·508 mm, $d/h = 0{\cdot}0067$) in the '2' intake, of static and total pressure, mass flow and total pressure efficiency with $m_1/m^* = 0{\cdot}710$ without blowing.

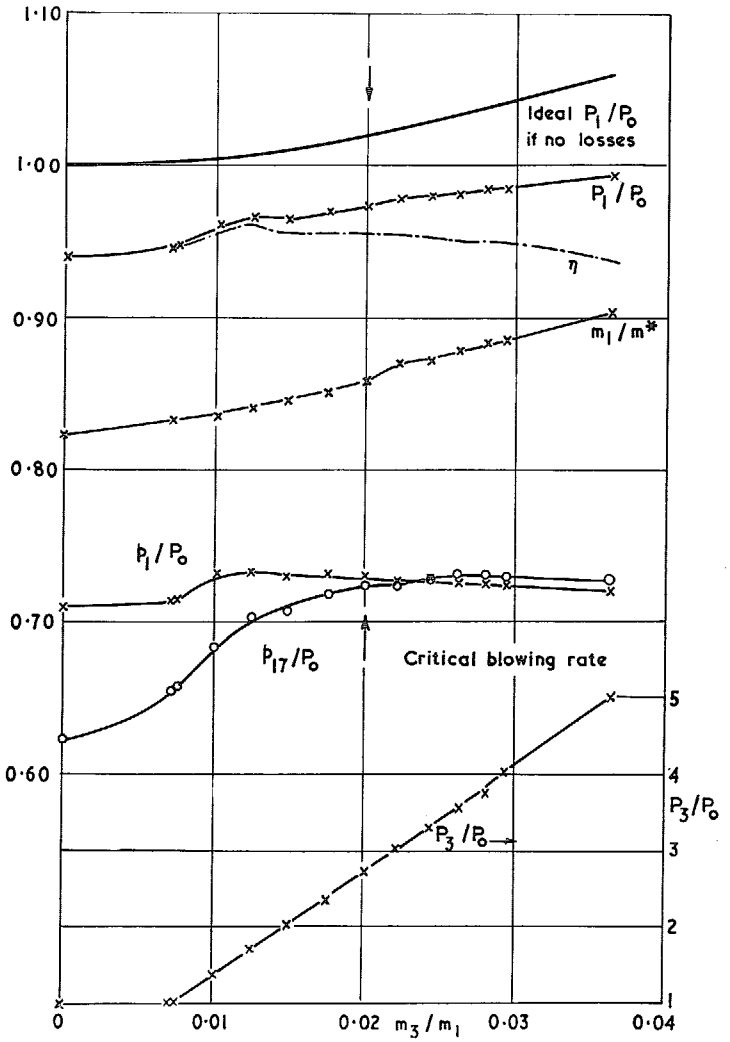

FIG. 20. Variation with blowing rate through a 0·020 in. slot (0·508 mm, $d/h = 0{\cdot}0067$) in the '2' intake, of static and total pressure, mass flow and total pressure efficiency with $m_1/m^* = 0{\cdot}823$ without blowing.

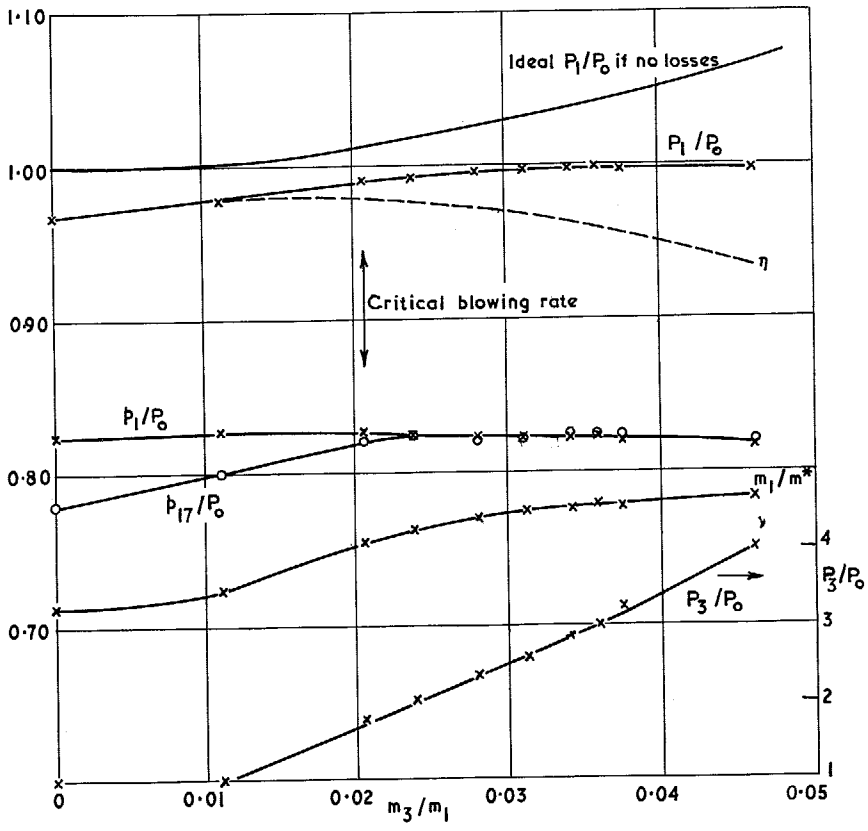

FIG. 21. Variation with blowing rate through a 0·030in slot (0·762mm, $d/h = 0{\cdot}010$) in the '2' intake, of static and total pressure, mass flow and total pressure efficiency with $m_1/m^* = 0{\cdot}71$, without blowing.

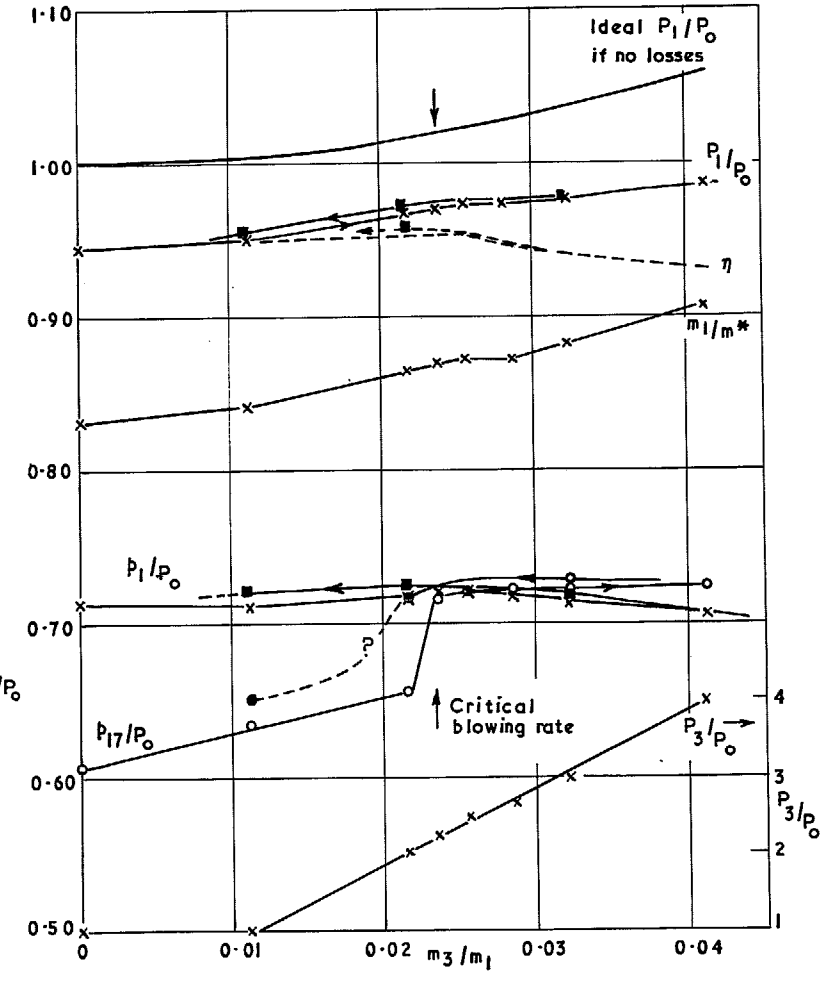

FIG. 22. Variation with blowing rate through a 0·030in slot (0·254mm, $d/h = 0{\cdot}010$) in the '2' intake, of static and total pressure, mass flow and total pressure efficiency with $m_1/m^* = 0{\cdot}83$ without blowing.

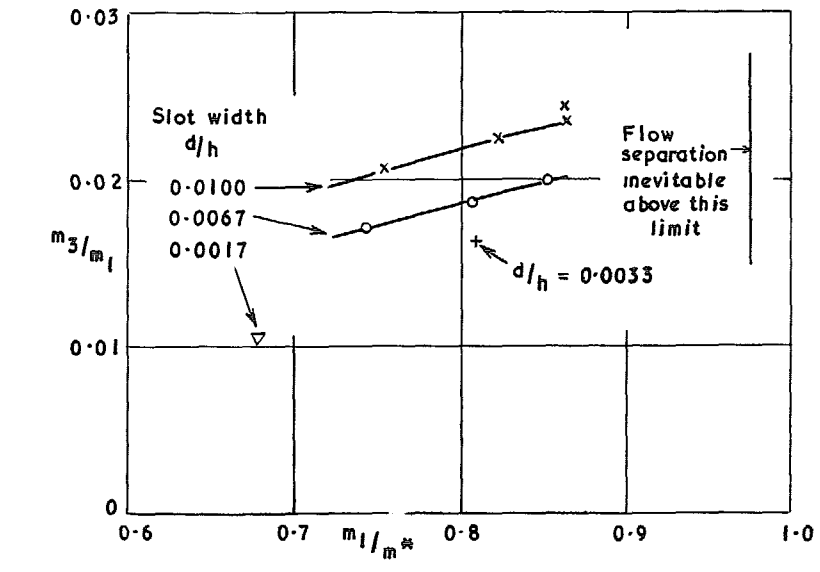

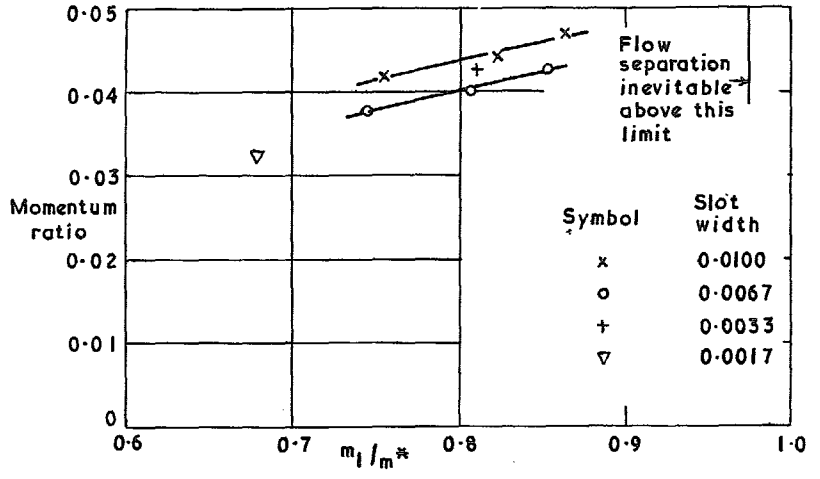

FIG. 23. Effect of slot width and intake mass flow on critical blowing mass flow and momentum ratios required just to prevent separation on '2' intake.

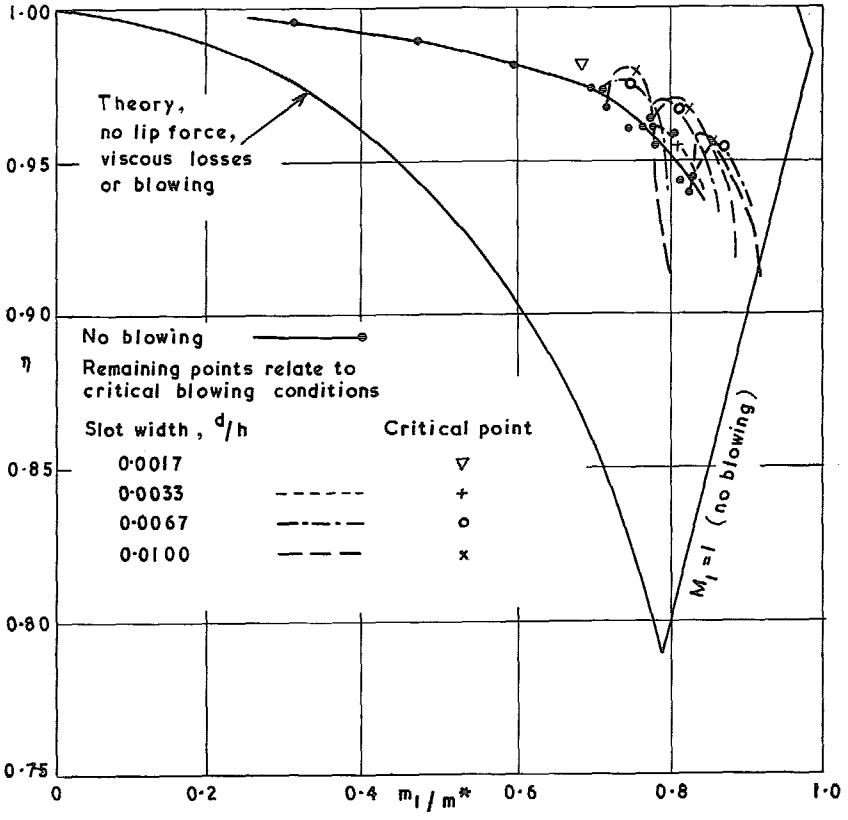

FIG. 24. Variation of total pressure efficiency of '2' intake with mass flow, with and without blowing. (Results with blowing are given at various constant iris valve settings).

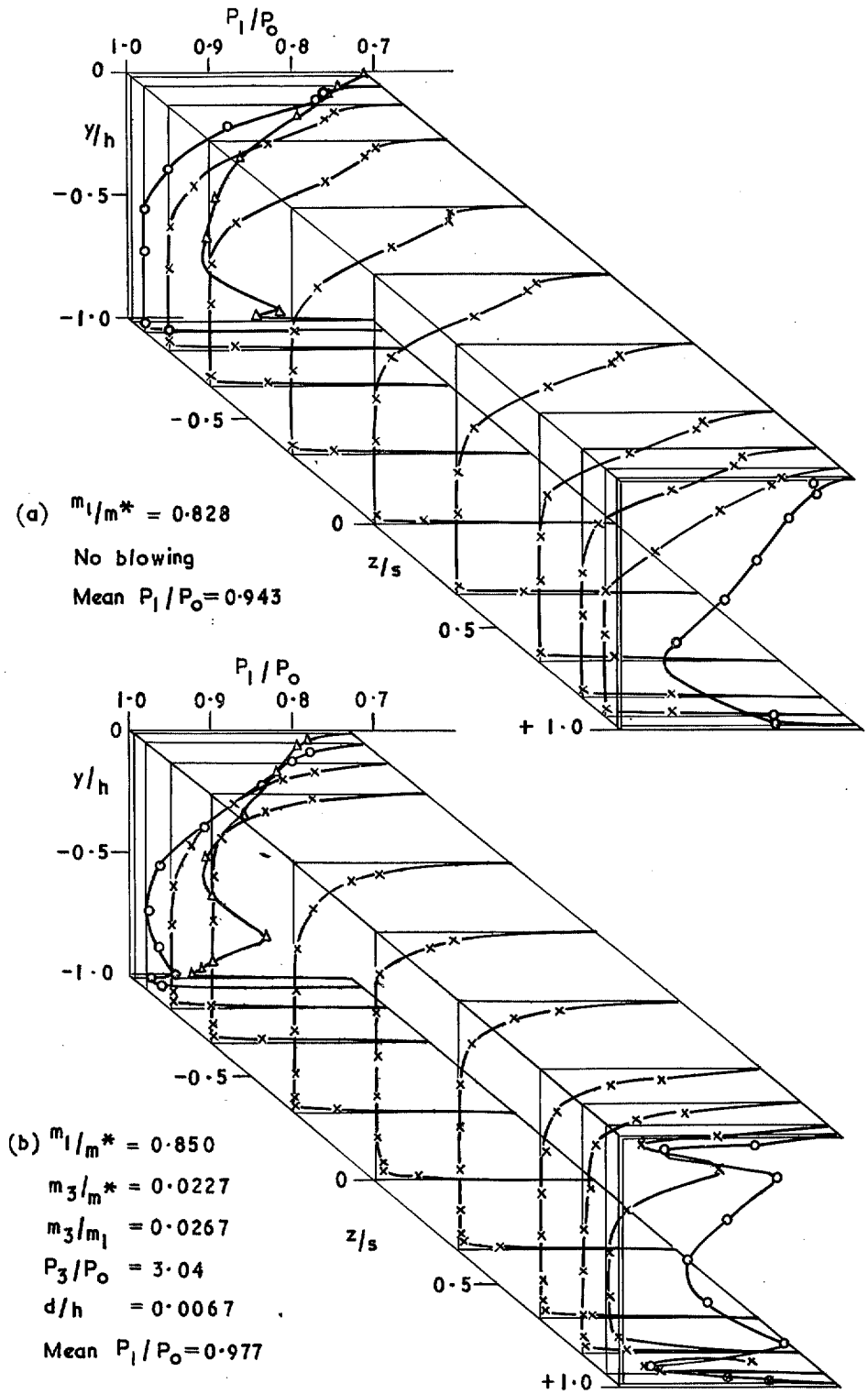

FIG. 25. Total pressure profiles in '2' intake, 1·67h downstream of slot lip, (a) without blowing (b) with blowing.

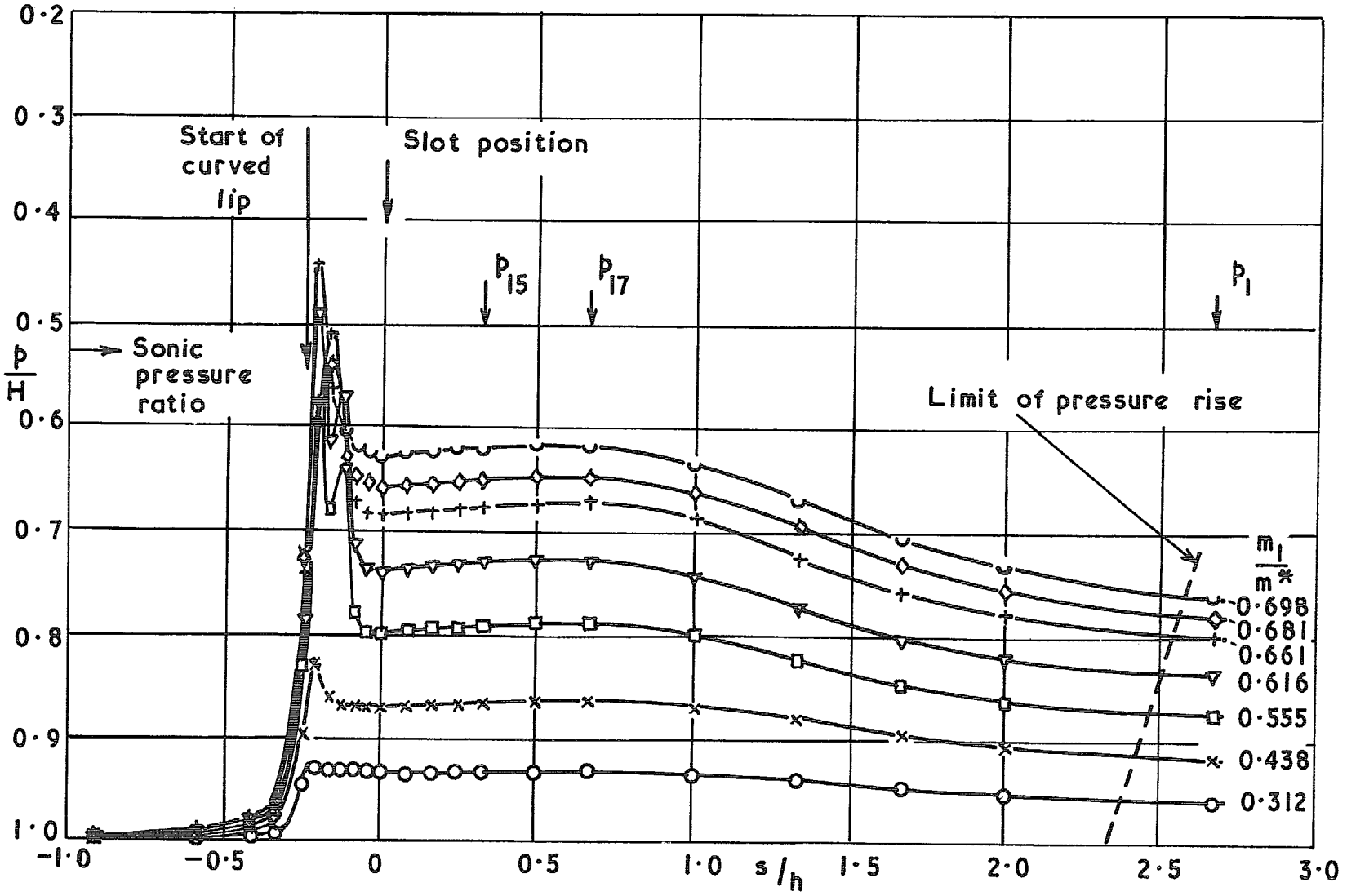

FIG. 26. Pressure distribution '$2\sqrt{2}$' intake without blowing.

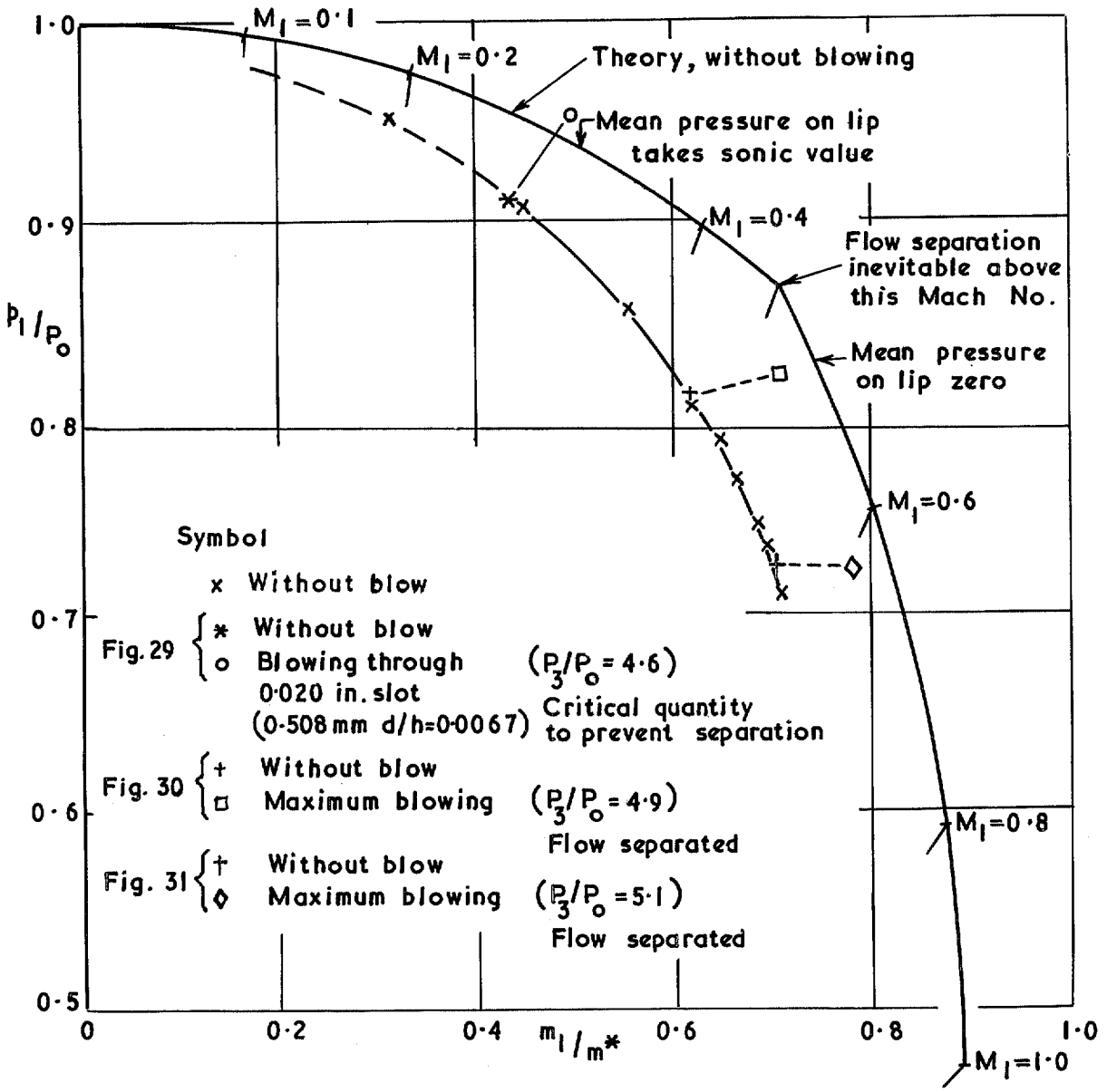

FIG. 27. Variation with mass flow of static pressure far down '$2\sqrt{2}$' intake, with and without blowing.

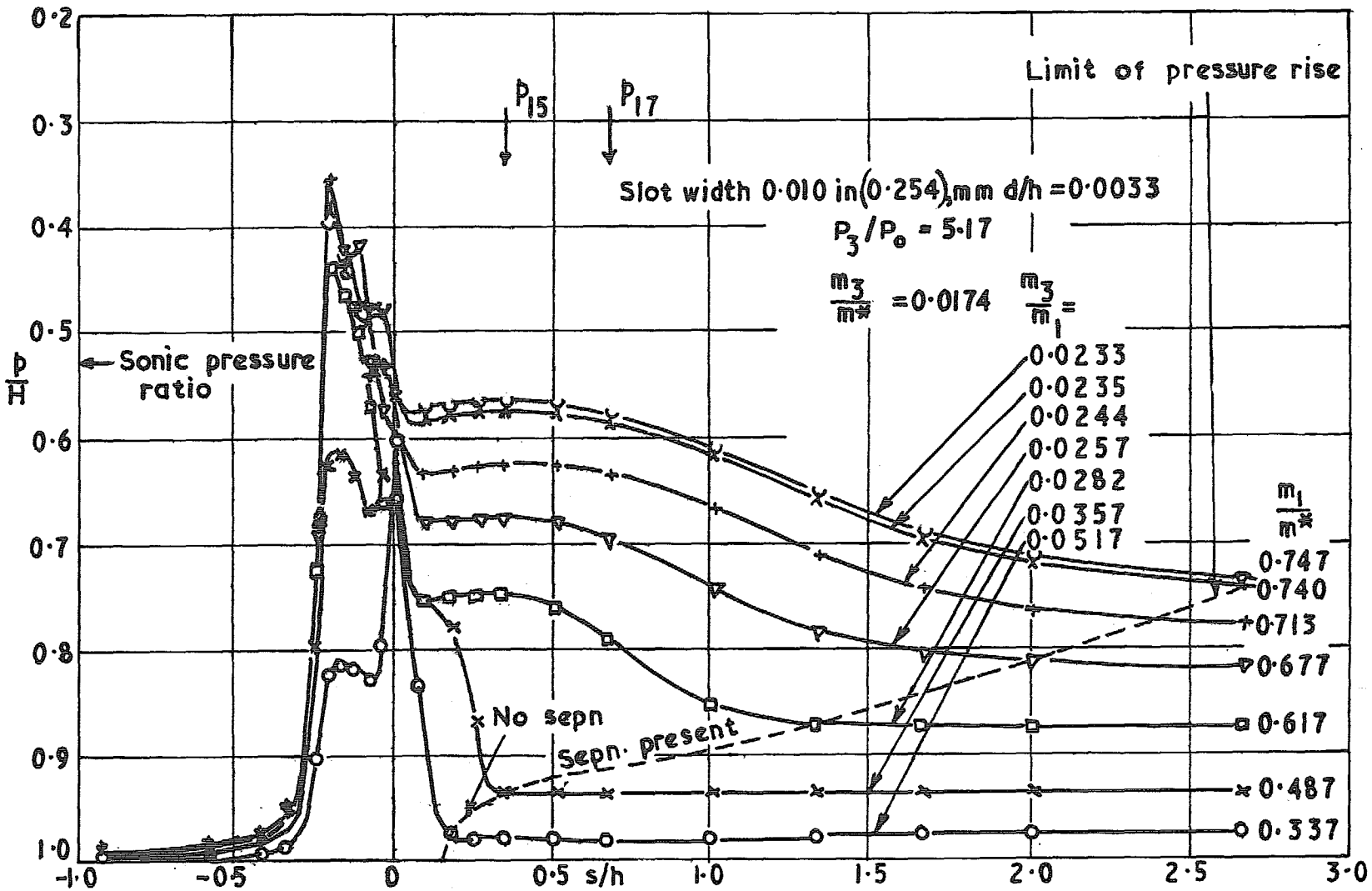

FIG. 28. Effect of constant blowing rate on pressure distribution on '$2\sqrt{2}$' intake.

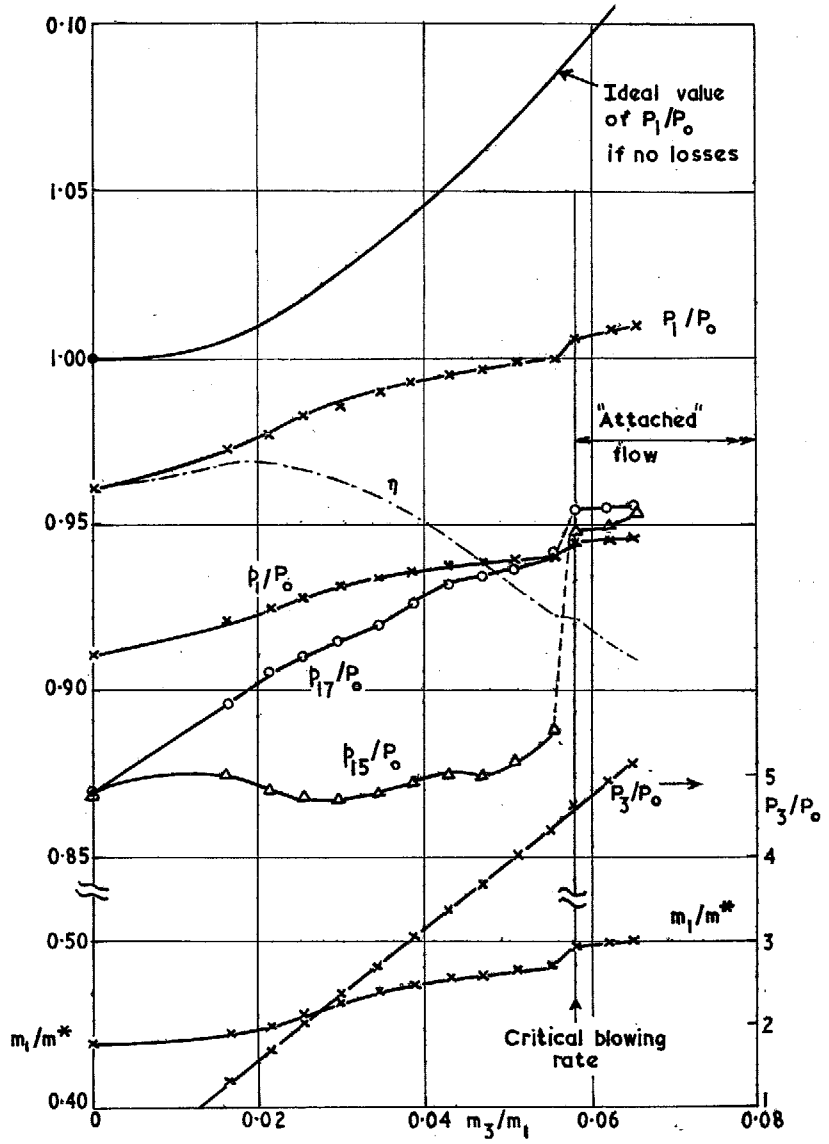

FIG. 29. Variation with blowing rate through a 0·020 in slot (0·508mm, $d/h = 0{\cdot}0067$) in the '$2\sqrt{2}$' intake of static and total pressure, mass flow and total pressure efficiency with $m_1/m^* = 0{\cdot}439$ without blowing.

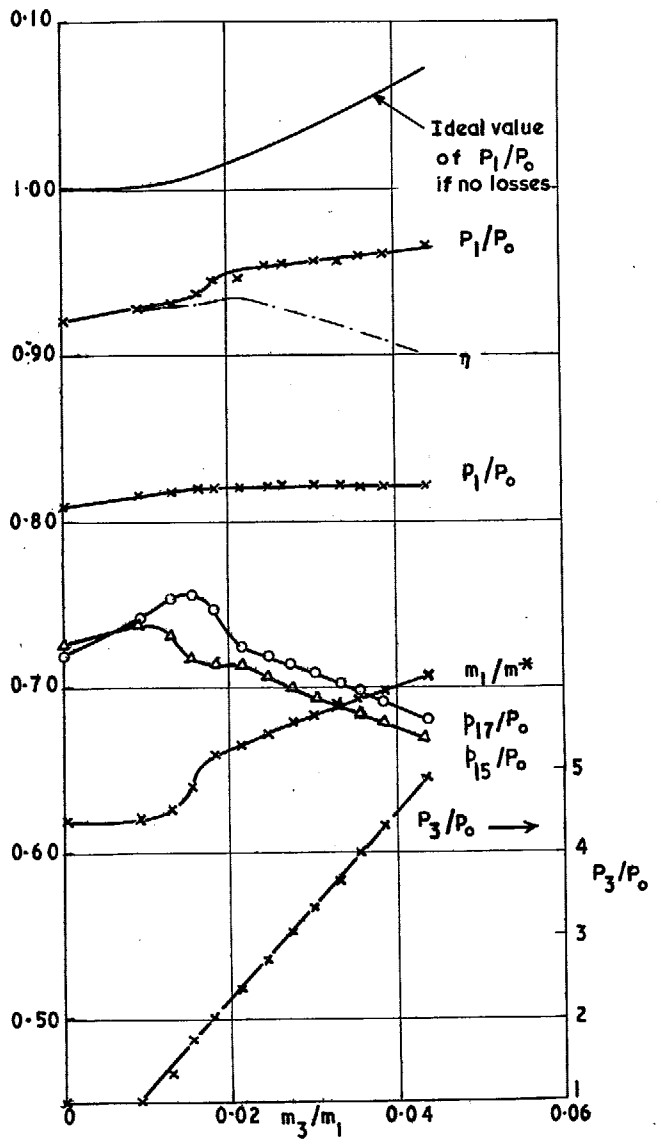

FIG. 30. Variation with blowing rate through a 0·020in slot (0·508mm, $d/h = 0{\cdot}0067$) in the '$2\sqrt{2}$' intake of static and total pressure, mass flow and total pressure efficiency, with $m_1/m^* = 0{\cdot}619$ without blowing.

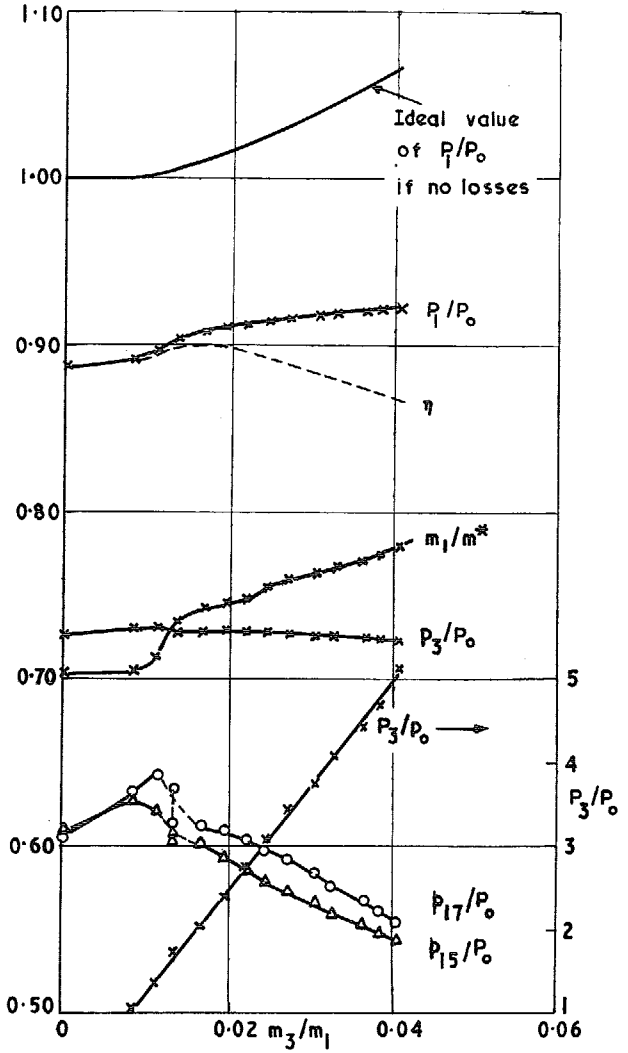

FIG. 31. Variation with blowing rates through a 0·020in slot (0·508mm, $d/h = 0{\cdot}0067$) in the '$2\sqrt{2}$' intake of static and total pressure, mass flow and total pressure efficiency, with $m_1/m^* = 0{\cdot}703$ without blowing.

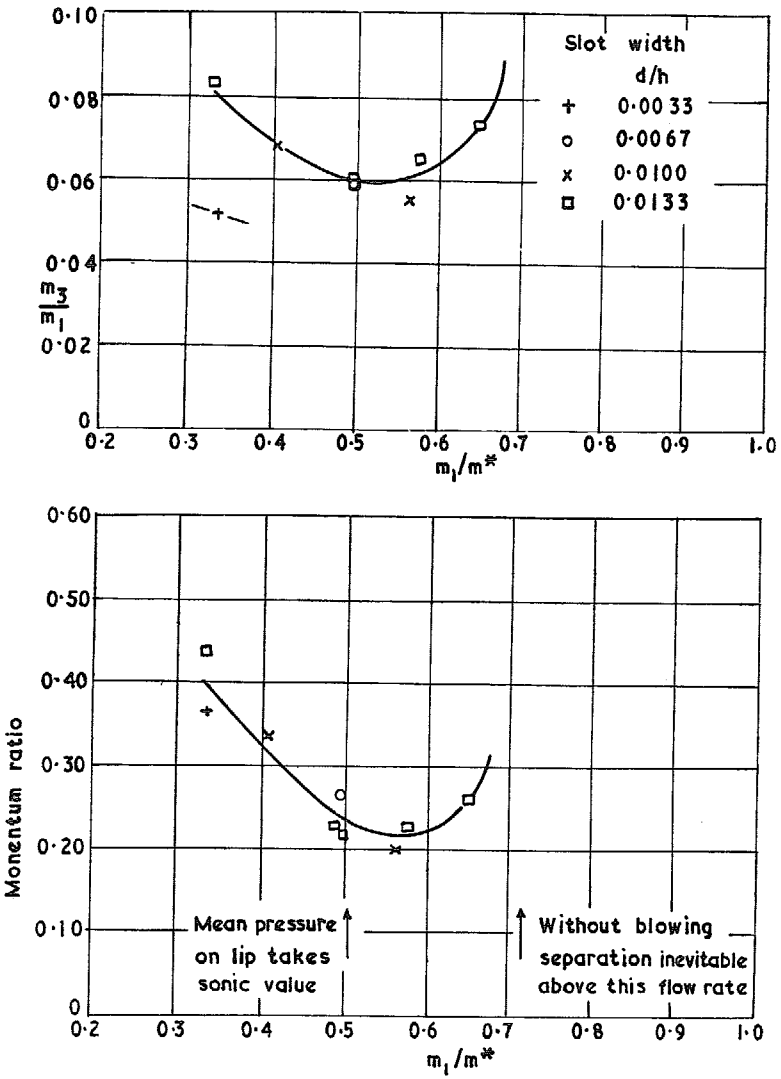

FIG. 32. Effect of slot width and mass flow on critical blowing mass flow and momentum ratio required just to prevent separation in '$2\sqrt{2}$' intake.

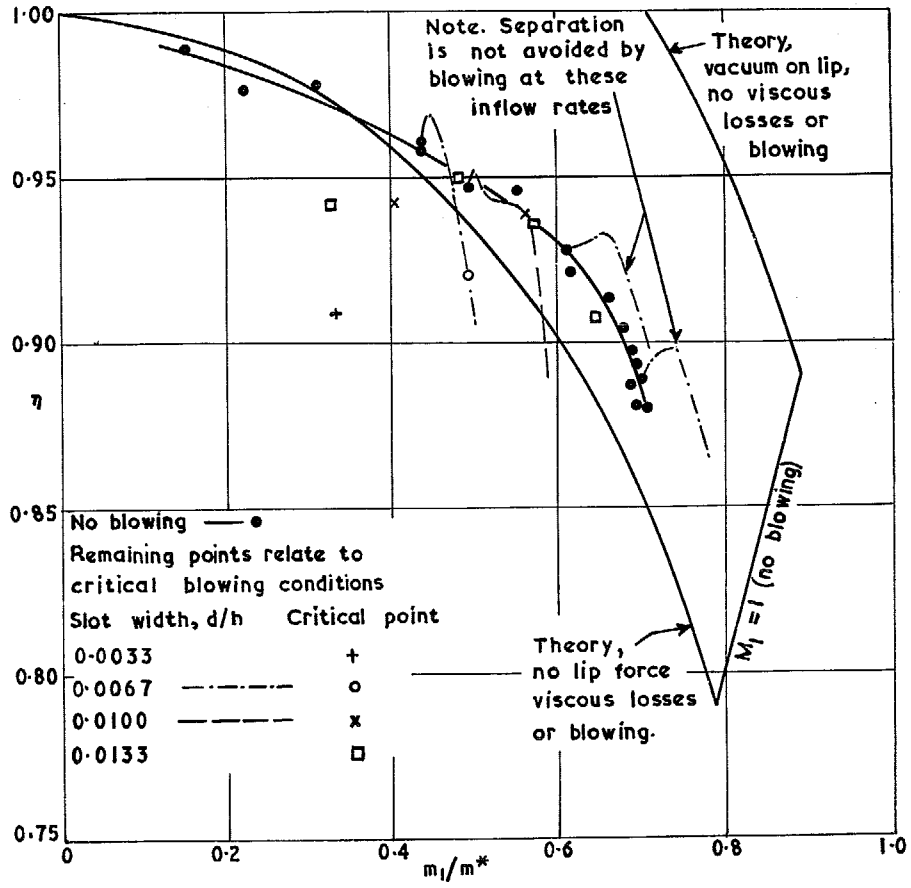

FIG. 33. Variation of total pressure efficiency of '$2\sqrt{2}$' intake with mass flow with and without blowing. (Results with blowing are given at various constant iris valve settings).

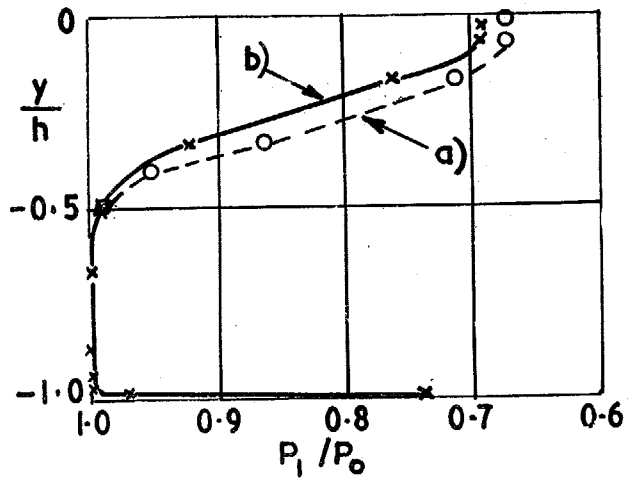

FIG. 34. Total pressure profile in '$2\sqrt{2}$' intake at mid-span station, 1·65h downstream of slot slip.
(a) without blowing, $m_1/m^* = 0{\cdot}708$. Mean $P_\perp/P_0 = 0{\cdot}893$ (mid-span).
(b) with (sub-critical) blowing, $m_1/m^* = 0{\cdot}755$, $m_3/m^* = 0{\cdot}0174$, $m_3/m_1 = 0{\cdot}0231$, $P_3/P_0 = 5{\cdot}23$, $d/h = 0{\cdot}0033$. Mean $P_1/P_0 = 0{\cdot}912$ (mid-span).

Printed in Wales for Her Majesty's Stationery Office by Allens Printers (Wales) Limited
Dd. 501372 K.5

Published by
HER MAJESTY'S STATIONERY OFFICE

To be purchased from
49 High Holborn, London WC1V 6HB
13a Castle Street, Edinburgh EH2 3AR
109 St Mary Street, Cardiff CF1 1JW
Brazennose Street, Manchester M60 8AS
50 Fairfax Street, Bristol BS1 3DE
258 Broad Street, Birmingham B1 2HE
80 Chichester Street, Belfast BT1 4JY
or through booksellers

R. & M. No. 3656

SBN 11 470376 0